View metadata, citation and similar papers at core.ac.uk

brought to you by CORE

provided by NASA Technical Reports Server

General Disclaimer

One or more of the Following Statements may affect this Document

- This document has been reproduced from the best copy furnished by the organizational source. It is being released in the interest of making available as much information as possible.

- This document may contain data, which exceeds the sheet parameters. It was furnished in this condition by the organizational source and is the best copy available.

- This document may contain tone-on-tone or color graphs, charts and/or pictures, which have been reproduced in black and white.

- This document is paginated as submitted by the original source.

- Portions of this document are not fully legible due to the historical nature of some of the material. However, it is the best reproduction available from the original submission.

Produced by the NASA Center for Aerospace Information (CASI)

(NASA-CR-144932) A STUDY OF FATIGUE CRACK CLOSURE USING ELECTRIC POTENTIAL AND COMPLIANCE TECHNIQUES (Boeing Co., Wichita, Kans.) 43 p HC $4.00 CSCL 13M

N76-19483

Unclas
G3/39 20725

NASA CR-144932

A STUDY OF FATIGUE CRACK CLOSURE USING ELECTRIC POTENTIAL AND COMPLIANCE TECHNIQUES

BY C. K. CLARKE AND G. C. CASSATT

PREPARED UNDER CONTRACT NO. NAS1-13881

THE BOEING COMPANY
WICHITA DIVISION
WICHITA, KANSAS

FOR

NATIONAL AERONAUTICS AND SPACE ADMINISTRATION

TABLE OF CONTENTS

LIST OF TABLES

LIST OF FIGURES

LIST OF SYMBOLS

S_{max}	Maximum gross section stress
S_{min}	Minimum gross section stress
S_{op}	Stress at which the crack opens on loading
U	Effective stress ratio (defined in Equation 1)
K	Stress intensity
K_{max}	Maximum stress intensity
H	Height of compact tension specimen
W	Width of compact tension or panel specimens
B	Thickness of specimens
R	Stress ratio, S_{min}/S_{max}
a	Half crack length for center cracked specimens and full crack length for edge cracked specimens
Ω	Resistance
ρ	Resistivity
ℓ	Length of conductor
A	Cross-sectional area of conductor
E	Electric potential
I	Current
σ_{net}	Net section stress

A STUDY OF FATIGUE CRACK CLOSURE USING ELECTRIC POTENTIAL AND COMPLIANCE TECHNIQUES

By C. K. Clarke and G. C. Cassatt

THE BOEING COMPANY
Wichita Division
Wichita, Kansas

SUMMARY

The objective of this work was to compare closure data produced on the same specimen by the crack tip compliance gage and electric potential techniques. Experiments on 7075-T651 aluminum center cracked panels produced equivalent results on closure using the two techniques. The results also indicated that closure is a function of stress ratio, specimen thickness and maximum applied stress intensity. Maximum stress intensity had a strong effect on closure in the range of applied stresses used. This dependence of closure on specimen thickness and maximum stress intensity accounts for many of the discrepancies in closure behavior reported in the literature.

INTRODUCTION

Fatigue in aircraft structures was first recognized as a problem during WWII, but did not receive serious attention until the British Comet aircraft failures in the early 1950s. Much effort has been devoted since that time to the study of fatigue. However, a basic understanding is still not available and present techniques to predict fatigue in aircraft structures are unreliable. Crack closure is one physical phenomenon associated with fatigue which accounts for some of the nonlinear behavior of crack growth. This report compares two techniques used to study closure.

Objective

The objective of this work was to study crack closure using compliance and electric potential techniques. Both techniques were to be compared by simultaneously recording both measurements. Additional efforts were also to be made for improved electric potential technique.

Background

Crack closure is the phenomenon where faces of a fatigue crack remain in contact during part of a fatigue load cycle. Crack tip deformation, hence crack extension, will not occur while the faces are in contact. Thus, the effective load range for crack growth is the total applied load range minus the load range over which the faces are in contact.

The phenomenon of closure was first observed by several investigators in the early 1960s using electric potential methods to study slow crack growth (References 1, 2, 3). The electric potential system was used to monitor specimen behavior while loading the specimen to failure. The resulting potential versus load curves exhibited an initial nonlinear segment followed by a linear segment. The initial nonlinear segment was considered evidence of crack closure.

Closure was not reported again until 1970 when Elber observed the phenomenon in the form of nonlinear displacements in a fatigue specimen being sectioned for fractography (Reference 4). Displacements were observed during the cutting of the specimen. Compressive loads were reapplied to the specimen and the displacements monitored. The resulting plot of displacement versus load was nonlinear and considered evidence of a changing specimen geometry. This was interpreted as a change in the effective crack length with changing load. Flattened fatigue striations, indicative of crack closure, were found during fractographic examination of the fatigue surfaces.

A comprehensive study of fatigue crack closure was undertaken by Elber (Reference 5) following his first brief observations. Center cracked panels of 2024-T3 aluminum (5 mm thick) were used in this study. A special crack tip compliance gage with a gage length of 1.5 mm was developed for accurate measurement of displacements near the crack tip. Closure was studied for R ratios ranging from −0.1 to 0.7 and stress intensity ranges of $13 < \Delta K < 40$ MN/m$^{3/2}$ at constant amplitude.

Elber characterized closure in this work in terms of an effective stress ratio, U, which is defined in Equation 1.

$$U = \frac{S_{max} - S_{op}}{S_{max} - S_{min}} \tag{1}$$

The term $(S_{max} - S_{op})$ reflects that closure decreases the effective load range for crack growth. Elber found the effective stress ratio, U, to be a function of the stress ratio R, but not of crack length. The experimentally determined relationship between U and R is given by Equation 2.

$$U = 0.5 + 0.4R \tag{2}$$

Tests with spike overloads and load changes were also run. The effective stress ratio decreased following the application of a single overload while an increase in the effective stress ratio was observed when the load was increased and cycling continued at the higher new load.

Elber's work spurred additional investigations by other researchers using approaches that broke down into two categories; surface measurements and bulk measurements. The results for each category are reviewed in the following paragraphs.

Surface measurements.— Measurements of surface displacements belong in this category and include strain gages, optical means of monitoring surface displacements, and Elber-type crack tip compliance gages.

N. J. I. Adams (Reference 6) studied closure in two specimens of 2024-T3 aluminum using photography to record displacements at the crack tip. The resuits show a decreasing U with increasing K_{max} (K_{max} increased due to crack length). Low K_{max} values, 3.4 MN/m$^{3/2}$ were used in this study.

Roberts and Schmidt (Reference 7) developed a strain gage technique to study closure. A strain gage was placed over the crack tip so that only the ends of the gage were bonded leaving the center section unrestrained. These gages were applied to compact tension specimens made from 2024-T3 (B = 3.2 mm) and 7075-T6 (B = 6.35 mm). Other specimen dimensions were H/W = 0.6 and W = 63.5 mm. This specimen and gage arrangement produced U = 0.8 for R = 0 and K_{max} values of 8.8 to 16.5 $MN/m^{3/2}$ in both specimens in contrast to U = 0.5 found by Elber.

Sharp and Grandt (Reference 8) used a laser interferometry technique which produced 0.1 micron displacement resolution to monitor crack tip displacements in 2024-T851 compact tension specimens (B = 25.4 mm). They found an effective stress ratio of 0.82 (R = 0.1) using the interferometry technique as opposed to 0.54 predicted by Elber. Crack tip strain gages, similar to those used by Roberts and Schmidt, were also used. Crack opening loads, approximately half of those observed with the strain gages, were recorded using the laser method. The laser method showed an immediate increase in the crack opening load after the application of an overload. This again conflicted with Elber's observation of a slowly increasing crack opening load.

Frandsen, Inman and Buck (Reference 9) compared the results of Elber's crack tip compliance gage with those from an acoustic emission technique on through cracked and compact tension specimens of 2219-T851. The acoustic technique was used on both specimens while compliance gages were used on the compact tension specimens only. Good agreement existed between the two techniques at low R values. However, they found the onset of closure difficult to ascertain with the Elber gage at higher R values. Closure was not seen at R = 0.5 with the Elber gage, while the acoustic technique showed closure. These authors found that U increased with K_{max} starting at low K_{max} values and finally became constant at K_{max} = 10 $MN/m^{3/2}$. A difference in U between 7075 and 2219 alloys was noted (factor of approximately 1.7), and specimen geometry also had an apparent effect on U.

Bulk measurements.— Acoustic, potential and photoelastic measurements are considered to represent bulk behavior as opposed to surface behavior measured by the previously described approaches. Different stress states in the bulk and surface could produce different closure results; therefore, the two approaches might be expected to yield different results.

Several investigators (References 1, 2, 3) observed the closure phenomenon while studying stable cracking with potential systems. Electric resistance or potential systems were used to monitor crack growth in specimens underload. Changes in resistance or potential occur with changes in crack length because the length of the current path increases with load. The investigators found that resistance-versus-load curves produced by loading a specimen to failure were initially nonlinear followed by a linear change in resistance with load. Depending on the toughness of the material, the curves became nonlinear again prior to fracture, or the specimen broke in the linear region. The initial nonlinearity was attributed to crack faces that initially closed and then opened with rising load. The linear region of the resistance-versus-load relationship was indicative of elastic loading, and the nonlinearity prior to fracture was considered evidence of gross specimen plasticity.

A value for U can be estimated from some of the data (Reference 1) by taking the maximum precracking stress as not less than half the breaking stress and no greater than the stress at the upper limit of the linear region of the curve. The U for a 2 mm thick center cracked specimen of 300M steel thus calculated ranges from 0.61 to 0.71 (at R = 0) for these two limits.

Shih and Wei (References 10, 11) used a dc potential system to study closure in mill annealed Ti-6Al-4V alloy plate material. Center cracked panel specimens (B = 5.08 mm) were used for this study with R ratios of 0.1 to 0.5 and K_{max} values of 16.5 to 44 $MN/m^{3/2}$. U ranged from 0.63 to 0.93 at R = 0.1 for decreasing K_{max} and was equal to 1.0 for all K_{max} at $R \geq 0.3$. This trend in U with K_{max} was the opposite of that reported by Frandsen, Inman and Buck (Reference 9). Shih and Wei also had difficulty measuring closure at short crack lengths. Since varying K_{max} was achieved by increasing the crack length at constant load, it is not obvious whether a K_{max} or a 2a/W ratio effect was being observed. A crack tip strain gage of the type used by Roberts and Schmidt (Reference 7) was tested for comparison and produced results basically in agreement with the potential data.

Photoelasticity is a technique placed in the bulk category because of the capability to make observations perpendicular to the plane of the fatigue crack in addition to side measurements. Cheng and Bruzzone (Reference 12) used photoelasticity to study crack closure in a 3.2 mm thick edge cracked polyester resin specimen. A crack was grown for a distance and then the specimen was unloaded and photographed from the side. Fringes, inclined back toward the crack origin at the crack tip, were observed and taken as evidence that the crack faces were in contact at zero load. The highest compressive stresses were found near the crack origin.

Pitoniak, et al (Reference 13), used compact tension specimens (H/W = 0.8 and B = 17.8 mm) of polymethylmethacrylate (PMMA) and photoelasticity to study closure as a function of specimen thickness. The illuminating lamp was mounted on top of the specimen so that the light beam was perpendicular to the plane of the fatigue crack. They found that only the perimeter of the fatigue crack was closed or in contact at zero load. The center region of the crack actually separated. The crack faces were found to start separating at the midpoint of the crack starting saw cut and opened on loading along the fatigue crack perimeter.

A third bulk technique, ultrasonics, was used by Buck and coworkers to study closure (References 9, 14, 15) in 2219-T851 compact tension and part through cracked specimens. Two ultrasonic transducers were mounted on the back of the specimens to determine an effective crack length. Closure was determined from plots of apparent crack length versus load. They found U to be constant at 0.85 for R = 0.25 to 0.55 using an intercept method to interpret the data. However, their data show U increasing from 0.30 to 0.62 for increasing R for the same data when the point of closure is the point at which the crack length (ultrasonic signal) versus stress curve became linear. The stress where the curve became linear was nearly constant for all R ratios. The point at which the crack length versus stress curve became linear was a function of applied stress cyclic frequency with higher frequencies moving the point closer to the extrapolated point.

An analytical approach to studying closure is possible using finite element analysis methods. Although it is not an experimental technique, finite element analysis results are included at this point for comparison with the experimental results. Newman and Arman (Reference 16) developed an analysis to study closure analytically. Their analysis showed that higher gross section stresses produced lower U values. There was a difference in the crack opening load behavior as a function of cycles from starting for the two stress levels studied. Closure was not found for R = 0.5 at relatively high max stresses. Residual crack tip displacements plots indicated that residual deformation in the faces of the fatigue crack was responsible for closure.

PROCEDURE

Background on the potential system and details of the experimental procedure will be presented in this section.

Electric Potential Technique

The potential technique for measuring crack length and studying closure depends on two concepts:

a. The resistance (hence potential because E = IΩ) of a fatigue specimen depends on the specimen geometry. Resistance is proportional to the length of the current path, ℓ, through the remaining ligament and cross-sectional area, A, of the ligament as given by Equation 3. Thus, ℓ increases and A decreases as crack length increases.

$$\Omega = \rho \frac{\ell}{A} \tag{3}$$

b. The crack disturbs the potential field in the specimen in a manner analogous to cracks disturbing a stress field. Thus, crack length as a function of potential field can be derived.

Gilbey and Pearson (Reference 17) provide an analysis for the effect of position of the potential leads and the type of current supply contacts used on the sensitivity of potential crack length measurements. Their analysis showed that opposed centerline point contacts for the current supply provided two to three times more sensitivity than bus bar type contacts. They also found that greater sensitivity would be gained by placing the potential leads at the crack tip. The next best location was the centerline of the specimen as near the crack plane as possible.

There are three basic problems associated with the potential technique for studying closure:

a. A high current density should exist at the crack tip and some crack tip heating could thus be expected. The effects of a high crack tip current density may be offset by local increases in resistance at the crack tip because of heating resulting in lower crack tip current densities.

b. The freshly created crack surfaces must be protected from oxidation to prevent electrical insulation of these surfaces, and consequent masking of closure effects (Reference 10).

c. A noise-sensitivity problem exists. Electronic noise was a serious problem, since the total closure signals measured in this study were often on the order of 1 microvolt. Noise and short crack lengths can combine to produce a situation where the system cannot detect closure with available currents. Higher currents would exceed power supply capacity or produce unacceptable specimen heating.

A dc potential system shown in Figure 1 was chosen for this study because of proven reliability. Electronic noise in the system was reduced by using an isolation transformer to isolate all control, recording, and amplifier equipment except the power supply. Further noise reductions were achieved by using spot-welded 2014 aluminum leads on the specimen to eliminate contact

noise and thermoelectric emfs. Going from bar-type power supply contacts to point contacts reduced current requirements by a factor of five. This permitted a smaller and more stable power supply to be used for additional noise reduction. Phenolic sleeves 1.6 mm thick were used over the loading pins along with phenolic spacers on the sides to insulate the specimen from the loading system.

Experimental Procedure

The material and specimen design used will be described in this section. Details of the environmental system and operating procedure will be provided also.

Material.— 7075-T651 aluminum in thicknesses of 6.4, 12.7 and 25.4 mm was used for this study. The plates from which the specimens were taken had a nominal yield stress of 552 MN/m^2 and ultimate strength of 607 MN/m^2.

Specimen Design.— The center cracked panel specimen was chosen because of its simplicity and analytical solutions available for potential as a function of 2a/W (References 17, 18). Single pin loading was selected to facilitate specimen removal from the chamber. Specimen dimensions (Figure 2) were chosen to conserve material and yet produce uniform stresses in the gage section (Reference 19). However, a problem with cracking in the load pinhole was experienced with the specimen design which required a specimen design modification part way through the program. The specimen width was changed as shown in Figure 3 to eliminate the cracking problem.

Several types of potential leads and methods for attachment to the specimen were tried prior to the closure tests. The best arrangement was aluminum tape spot welded to the specimen. Other attaching techniques produced contact problems and anything but aluminum leads on aluminum specimens produced severe thermoelectric emf effects. Final placement of potential leads as shown in Figure 4 was also dictated by considerations of lead and crack tip gage interference. Potential leads were placed on the specimen centerline to prevent interference with the Elber gage. The power leads were placed as close to the crack as practical without interfering with the compliance gage and potential leads.

Environment system.— Figure 5 shows the environment system used to prevent oxidation of the crack faces. Linde high purity liquid argon (at least 99.998 percent) was used to provide an inert atmosphere. However, this gas alone was not sufficiently free of oxygen to permit detection of closure by the potential system. The addition of a titanium sublimation pump to the system (TiBall from Varian) reduced the oxygen level to the point where the oxidation rate was low enough to permit closure observations. Shih and Wei (Reference 10) referenced earlier work which showed that this approach could yield the equivalent oxygen content of a hard vacuum (2×10^{-7} torr).

Operating procedure.— The task of comparing measurements from the Elber crack tip gage with measurements obtained using the electric potential technique created two problems.

a. The gage had to be seated in position using 1/64 diameter drill holes for the point seats. The fatigue cracks then tended to aim towards the gage holes if the gage was located more than 2 mm ahead of the crack tip. Therefore, the gage had to be positioned after growing the crack to near the desired length.

b. Since two 2a/W crack lengths were to be studied, the specimen had to be removed from the chamber and the gage repositioned at the new crack length. Each crack length observed was a separate experiment.

Each experiment was started by saw cutting a crack starter slot with a jewelers saw to within 5 mm (2a) of the desired crack length. A fatigue crack was then started in air and grown 2.5 mm. The compliance gage was placed so the crack would run between the gage points. The specimen was then placed in the environmental chamber and the wiring connected. Argon flow and the cold traps were started after closing the chamber. The titanium sublimation pump was started one hour after starting the argon flow and was allowed to run for an hour before starting crack growth. A plot of compliance and potential was also run before starting crack growth in the oxygen-free environment.

The crack was grown approximately 2.5 (2a) mm (crack length measurements were made by a traveling microscope) in the environment, and compliance and potential plots were made. (A K_{max} of 10 $MN/m^{3/2}$ was the target for most crack growth.) If the compliance and potential plots produced indication of closure, digital data were taken. If not, the crack was grown several hundred cycles more until good measurements of closure could be obtained. The crack was then grown another 2.5 mm and measurements repeated. This second growth ensured that the crack tip was near the compliance gage. After all other tests, higher loads were sometimes run at the second crack length to study the effect of higher loads on closure at constant 2a/W and stress ratio. After all tests were complete, the specimen was removed and saw cut to the second length and the process started over again.

RESULTS

Determining Closure from Compliance and Potential Data

Compliance.— Closure was determined from digital compliance data by subtracting the slope of the initial part of the unloading curve from the original data. A least squares straight line was fitted to the first five unloading points of compliance gage output-versus-load data and the resulting equation differentiated to determine the slope. A full cycle of compliance gage output data was then analyzed by fitting a second-degree polynomial to succeeding groups of five data points. The previously determined linear slope was subtracted from the slope of the calculated polynomial at the midpoint (third datum point). The results were then integrated and plotted as load versus modified compliance gage output (Figure 6). Closure was identified as the point at which the resulting curve became linear on loading (or no change in modified compliance).

Potential.— Finding the crack opening load in the potential-versus-load data was not straight forward. Figure 7 shows a typical compliance gage and potential versus load plot. Good digital potential data was difficult to obtain as will be explained later.

Four regions can be seen in the high gain potential curve:

a. The potential is constant with increasing load in Region I. No crack opening occurs in this region.

b. The crack begins to open in Region II and the resulting change in potential with load is nearly linear.

c. Region III may or may not be linear and is apparently a transition region between Regions II and IV. Compliance data always indicates a fully open crack in part of this region so the mechanism involved is not closure alone. Later discussion will provide evidence that the potential system was sensitive to elastic dimensional changes and plastic deformation. These factors probably account for the problematical Region III.

d. Region IV represents a steady state, crack fully open condition. Thus, extrapolation of the second and fourth stages should produce the actual crack opening load. Comparison of results with concomitant compliance data support this procedure.

Review of Data

The electric potential and Elber-type crack tip compliance gage produced comparable closure results as shown in Figure 8 when optimum potential techniques were used. In addition, results on the functional relationship of closure with R, B and K_{max} were obtained. Closure had a functional relationship with R (Figures 9A and 9B) in this study different from that found by Elber (Reference 5). The effective stress ratio also depended on specimen thickness "B" as shown in Figure 10 and K_{max} as shown in Figure 11. The results in Figure 11 also reflect the influence of specimen thickness. A complete tabulation of data is given in Table I, and more details of the individual tests are given in the following paragraphs.

B = 12.7 mm, varying R.— Closure testing started with a specimen at R = 0. Tests at two crack lengths and constant K_{max} revealed no dependency of U on 2a/W. Typical plotted data are shown in Figure 7. Compliance gage data (at a different crack length) with the elastic unloading linearity subtracted for greater sensitivity are shown in Figure 6. Unusual problems were not encountered except the potential closure indications occasionally disappeared and then reappeared.

Lower gain settings were used most of the time in this and following experiments because the potential closure results at first appeared to be more easily interpreted. The importance of the detail in the potential signal was not appreciated until later. Thus it was difficult to go back and find the two separate regions in the low gain data. This fact accounts for some disagreement between the two techniques as seen in Figure 8.

The second specimen was run under conditions of R = 0.2. Closure again did not depend on 2a/W, but a dependency on K_{max} became apparent. First curves at the short crack length, 2a/W = .2, exhibited a hump in the loading curves for the potential data (Figure 12). This hump persisted until the minimum load on the specimen was dropped to zero. Subsequent testing at R = 0.2 revealed normal potential behavior similar to that found in Figure 7.

The potential signal disappeared again at a longer crack length. This time, potential behavior was monitored during unloading to zero load. Figure 13 shows two cycles of the R = 0 loading. The steep rise in potential and the overshoot is similar to that expected of a protuberance on the fatigue crack surface which effectively props the crack open. Such a protuberance (approximately 0.5 x 1.5 mm) was found on one of the crack faces at the end of the test.

Additional tests were run on the R = 0.2 specimen to determine the effect of K_{max} at constant 2a/W on closure. A slight increase in U was found on increasing K_{max}. The tests also revealed that the potential system was sensitive to changes in loading as shown in Figure 14. A load change destroyed the potential closure signal for over 100 cycles. After at least 400 cycles, the potential system returned to normal behavior. Compliance data on the same plot also showed a loss of closure in the first few cycles after the load increase.

The R = 0.2 specimen was unloaded and the crack tip gage removed for the last test on the specimen. With the potential system monitoring specimen behavior, the specimen was loaded to failure as shown in Figure 15. The initial loading behavior is indicative of "pop-in" fracture, which suggests that dropping to zero load locally welded areas on the crack face.

Potential closure measurements were difficult to obtain at short crack lengths under R = 0.5 conditions. At longer crack lengths, closure measurements were obscured by electronic noise as shown by Figure 16. Good closure data, by contrast, were obtained at short and long crack lengths by the crack tip compliance gage. Typical results are shown in Figure 17.

A second R = 0, B = 12.7 mm specimen was tested without the crack tip compliance gage to permit achievement of longer actual fatigue crack lengths in the oxygen-free environment. There was concern that such a specimen might produce closure results different from the others where the actual fatigue crack length was small (because of sawcutting). Closure was not seen in this specimen with the potential system until 2a/W = 0.26 was reached. Good crack closure measurements were made from this crack length on. The resulting U values were higher than those previously recorded, but the K_{max} values were also lower.

This second R = 0 specimen also produced an additional finding. In this case, time spent at some constant load mean affected the potential output. The load controller system was constructed so that the system held at mean load whenever stopped. Stops were made frequently prior to recording data before this effect was known. The effect was seen in the data where the agreement between potential and compliance measurements was poor; long holds at mean load occurred before taking data.

Constant R, varying B.— Two specimens of thicknesses other than 12.7 mm were included in the test plan to investigate the effect of specimen thickness. These specimens could reveal differences, if they existed, between the two techniques used to study closure.

Closure could not be detected by the potential system in a B = 25.4 mm specimen because the specimen was too large. The power source available could not supply enough current for the sensitivity required to detect closure. The Elber gage detected closure and recorded a lower U value as shown in Figure 10.

The potential results from a specimen with B = 6.35 mm exhibited good sensitivity and low noise. Random noise was practically absent and high sensitivity was available. Typical results are shown in Figure 19. In this instance, no delays at positive loads were involved and U values for the compliance and potential systems agree well. The initial and final linearities in the potential data are seen clearly also. Figure 10 summarizes the results of the effect of thickness on U.

Smooth specimen.— A smooth specimen was tested in the form of an hourglass-shaped tensile specimen (Figure 20). This specimen produced a linear load-versus-potential output curve for elastic

loading. Total change in voltage measured was 0.25 microvolt for loading from 0 to 27.8 MN, which is close to a change of 0.8 microvolt predicted on the basis of elastic dimensional changes. Figure 21 shows the results for loading into the plastic range. A drop in potential was recorded each time specimen plasticity occurred. This same drop could be seen on a smaller scale near maximum load (on loading) in much of the fatigue specimen data.

DISCUSSION OF RESULTS

Specific observations on the potential technique for studying closure and the overall closure results are discussed in this section.

Potential System Behavior

The overall results show that the potential and compliance gage techniques for studying crack closure agree well within the data scatter (Figure 8). Under optimum conditions, the agreement was ±5 percent. Some specific observations on the potential technique are discussed specifically in the following paragraphs.

Hold at mean load.— The change in potential output caused by holding at positive loads accounts for the poor digital potential data frequently observed. Specimens were held at mean load while electrical connections were made, and time was required to make each digital reading at a given load. Time delay also affected many of the potential measurements. Later measurements, after discovery of the delay phenomena, show better agreement with compliance data because holds were reduced or eliminated.

There are two possible causes for the phenomena; oxidation and specimen time dependent behavior. The environmental system used provided a greatly reduced oxygen concentration, but one which was still considerably above equilibrium requirements for an oxide-free surface. Holding at loads which open the crack face would permit gradual oxidation and a gradual change in the potential signal.

The second possibility is time-dependent dislocation movement. This could affect resistivity in aluminum alloys and thus produce changes in potential measurement of closure or closure itself. The possibility also exists that oxidation and time-dependent plastic deformation act together to produce the changes seen when holding the load at a constant value.

Increases in load.— The compliance data was inadequate to fully determine if the compliance and potential systems behaved differently under changes in loading. Close examination of the data in Figure 14 suggests that both systems follow the same behavior in that U increases immediately with an increase in load.

Protuberances.— Protuberances on the crack surface were detected by the potential system. However, these protuberances obviously do not affect compliance gage behavior. The compliance gage data in Figure 13 still show some closure while the potential system indicates a fully open crack. This is puzzling since there should be some crack face area protected from oxidation when closure exists although most of the crack area could be oxidized. The potential system should be

sensitive to the remaining closed faces. This was the only case where the two techniques completely disagreed.

Smooth specimen results.– The smooth specimen showed that the potential system was sensitive to elastic changes in specimen dimensions and specimen plasticity. This fact is probably responsible for the third region in the load versus potential curves. The sharp drop in potential with plastic deformation is an interesting phenomenon and is thought to be the result of adiabatic heating produced by plastic deformation. The heating would produce an increase in resistance (and potential) and result in localized heating. A thermoelectric effect from the localized heating could then produce a larger negative potential change than that produced by the adiabatic heating and, thus, produce the observed drop in potential. More study is required to explain this observation.

Overall Results

The shape of the potential curve is complex and was not understood until the end of the program. Initial interpretation of the curves produced a constant U of approximately 0.8, regardless of conditions. After some study, it was found that the second and fourth regions, when extrapolated, gave a point of crack opening on loading which agreed with the compliance data. All data were then interpreted in this fashion with good results.

The final technique is defensible if the second region (Figure 7) is indicative of crack opening and the fourth region elastic-plastic loading. However, this leaves an undefined third region. The crack faces were always open during part of this stage, which indicates that more than closure is involved as a mechanism. The explanation for this region is not obvious, but the region appears to hold promise of revealing more information on crack tip behavior.

The strong effect of K_{max} on U is an important result of this research. The dependency of U on K_{max} explains inconsistencies in other published studies. The results of different specimen thicknesses and the effect of R in this study must be examined more closely since K_{max} varied in these experiments. Additional closure studies should be accomplished to further define this effect of K_{max} on U and to restudy other variables taking into account the strong effect of K_{max}.

CONCLUSIONS

The following conclusions were reached in this study of closure using electrical potential and compliance techniques:

a. The crack tip compliance gage and the electric potential techniques produce equivalent results on crack closure.

b. Closure depended on stress ratio R, specimen thickness B, and K_{max}. The dependence on K_{max} was quite strong and may have influenced the observations on the effects of R and B.

c. The potential technique for studying closure in aluminum requires an environment system and low noise, high gain data acquisition equipment. Experimental procedure is important also. Both factors combine to make the potential technique difficult to use for closure studies.

d. The potential technique may provide information on crack tip behavior in addition to closure observations.

e. More work on closure is necessary because of the strong effect of K_{max} on closure.

The Boeing Company,
Wichita, Kansas,
March 1, 1976

REFERENCES

1. E. A. Steigerwald and G. L. Hanna, "Initiation of Slow Crack Propagation in High Strength Materials," Proc. Am. Soc. Testing Mat., Vol. 62, 1962, pp. 885-913.

2. A. A. Anctil, E. B. Kula, and E. DiCesare, "Electric Potential Technique for Detecting Slow Crack Growth," Proc. Am. Soc. Testing Mat., Vol. 63, 1963, pp. 799-808.

3. J. E. Srawley and W. F. Brown, "Fracture Toughness Testing Methods," Fracture Toughness Testing and Its Applications, ASTM STP 381, A.S.T.M., Philadelphia, 1965, pp. 133-198.

4. W. Elber, "Fatigue Crack Closure Under Cyclic Tension," Eng. Frac. Mech., Vol. 2, 1970, pp. 37-45.

5. W. Elber, "The Significance of Fatigue Crack Closure," Damage Tolerance in Aircraft Structures, ASTM STP 486, ASTM, Philadelphia, 1971, pp. 230-242.

6. N. J. I. Adams, "Fatigue Crack Closure at Positive Stresses," Eng. Frac. Mech., Vol. 4, 1972, pp. 543-554.

7. R. Roberts and R. A. Schmidt, "Observations of Crack Closure," Int. J. Frac. Mech., Vol. 8, 1972, pp. 469-471.

8. W. N. Sharpe and A. F. Grandt, "A Preliminary Study of Fatigue Crack Retardation Using Laser Interferometry to Measure Crack Surface Displacements," presented at 8th Nat. Sym. on Frac. Mech., August 1974.

9. J. D. Frandsen, R. V. Inman, and O. Buck, "A Comparison of Acoustic and Strain Gage Techniques for Crack Closure," Int. J. Frac. Mech., Vol. II, 1975, pp. 345-348.

10. T. T. Shih and R. P. Wei, "A Study of Crack Closure in Fatigue," NASA CR-2319, 1973.

11. T. T. Shih and R. P. Wei, "A Study of Crack Closure in Fatigue," Int. J. Frac. Mech., Vol. 6, 1970, pp. 431-434.

12. Y. F. Cheng and H. Brunner, "Photoelastic Research in Progress on Fatigue Crack Closure," Int. J. Frac. Mech., Vol. 6, 1970, pp. 431-434.

13. F. J. Pitoniak, A. F. Grandt, L. T. Montulli and P. F. Packman, "Fatigue Crack Retardation and Closure in Polymethylmethacrylate," Eng. Frac. Mech., Vol. 6, 1974, pp. 663-670.

14. O. Buck, C. L. Ho, H. L. Marcus, and R. B. Thompson, "Rayleigh Waves for Continuous Monitoring of a Propagating Crack Front," Stress Analysis and Growth of Cracks, Proc. of the 1971 Nat. Sym. on Fracture Mech., Part I, ASTM STP 513, A.S.T.M., Phila., 1972, pp. 280-291.

15. O. Buck, C. L. Ho, H. L. Marcus, "Plasticity Effects in Crack Propagation," Eng. Frac. Mech., Vol. 5, 1973, pp. 23-24.

16. J. C. Newman and H. Arman, "Elastic Plastic Analysis of a Propagating Crack Under Cyclic Loading," 15th Structures, Structural Dynamics, and Mat. Conf., Los Vegas, 1974, AIAA Paper No. 74-366.

17. D. M. Gilbey and S. Pearson, "Measurement of the Length of a Central or Edge Crack in a Sheet of Metal by an Electric Res' ance Method," Royal Aircraft Establishment Tech. Rep. No. 66402, Dec., 1966.

18. H. H. Johnson, "Calibrating the Electric Potential Method for Studying Slow Crack Growth," Mat. Research and Stand., Sept. 1965, pp. 442-445.

19. W. G. Truckner, "Research on the Investigation of Metallurgical Factors on the Crack Growth Rate of High Strength Aluminum Alloys," Alcoa quarterly rep., August 1974, AFML Contract No. F33615-74-C-5079.

TABLE I
CALCULATED EFFECTIVE STRESS RATIOS

SPECIMEN	R	2a/W	POTENTIAL DIGITAL U	POTENTIAL PLOTTED U	COMPLIANCE-DIGITAL U	COMPLIANCE-PLOTTED U	K_{max} $MN/m^{3/2}$	σ_{net} MN/m^2	W mm
AFA-1	0	0.24	–	–	0.42	0.43, 0.48	9.42	79.98	63.5
B = 25.4 mm		0.28	–	–	0.59	0.43, 0.44	10.15	84.32	
		0.52	–	–	0.41	0.51, 0.51, 0.52	11.37	103.49	
		0.55	–	–	–	0.72, 0.71	17.44	165.33	
AFAK-6	0	0.26	–	0.70, 0.65	–	–	7.75	65.23	63.5
B = 12.7 mm		0.29	–	0.87, .83, .83 0.88	–	–	7.73	63.94	
		0.32	–	0.85 (.77)	–	–	7.93	65.27	
		0.36	–	0.82, 0.83	–	–	7.81	64.32	
		0.43	–	0.80, 0.83	–	–	7.50	63.38	
		0.52	–	0.85, 0.86	–	–	7.63	69.45	
		0.58	–	0.80, 0.84 0.85, 0.81	–	–	7.27	71.46	
AFAK-5	0	0.17	–	0.58	–	–	9.87	83.50	76.2
B = 12.7 mm		0.19	–	0.59	–	–	9.90	84.00	

Note: All of the effective stress ratios measured are tabulated in this table.
A dash line has been drawn where data was not available or interpretable.

TABLE 1. – Continued
CALCULATED EFFECTIVE STRESS RATIOS

SPECIMEN	R	2a/W	POTENTIAL DIGITAL U	POTENTIAL PLOTTED U	COMPLIANCE-DIGITAL U	COMPLIANCE-PLOTTED U	K_{max} $MN/m^{3/2}$	σ_{net} MN/m^2	W mm
AFA-3	0	0.22	–	0.54, 0.63	0.52	0.50, 0.51	11.46	99.43	63.5
B = 6.35 mm		0.26	–	–	0.63	0.65, 0.65	12.52	105.08	
		0.51	–	0.53, .55 0.55, .58	0.52	0.53, .53 0.54, .55	9.90	89.15	
		0.51	–	0.50, .56 0.48, .46, .47	0.63	0.62, .57 0.64, .60, .60, 0.63	17.34	157.21	
		0.56	–	0.47, 0.51 0.50 0.62, .62, 0.62, .63	0.58	0.58, .55 0.54 0.62, .63 0.58, .62	10.40	99.56	
		.56	–	0.76, .74 0.68, .69, .68	0.74	0.75 0.75, .71, .74	15.34	146.86	
AFAK-3	0	0.20	–	0.67, 0.70 0.74, 0.77	–	0.60, 0.53 0.57	10.67	86.19	76.2
B = 12.7 mm		0.52	–	0.68	0.68, 0.69	0.68	8.59	71.64	
		0.55	0.69, 0.69	0.59, 0.68	0.71, 0.70	0.71, 0.74	8.24	71.23	
		0.55	–	0.70, 0.73	–	0.74, 0.73	8.24	71.23	

Note: All of the effective stress ratios measured are tabulated in this table.
A dash line has been drawn where data was not available or interpretable.

TABLE 1. – Concluded
CALCULATED EFFECTIVE STRESS RATIOS

SPECIMEN	R	2a/W	POTENTIAL DIGITAL U	POTENTIAL PLOTTED U	COMPLIANCE-DIGITAL U	COMPLIANCE-PLOTTED U	K_{max} $MN/m^{3/2}$	σ_{net} MN/m^2	W mm
AFAK-10	0.2	0.22	–	–	0.90	0.82	11.21	88.76	76.2
B = 12.7 mm		0.22	–	.71, 0.78, .77	–	0.87, 0.89	11.21	88.76	
		0.52	–	0.76, 0.68, 0.77	0.78, 0.78	0.5C, 0.50	10.65	88.78	
		0.55	–	–	0.78	0.63, 0.61	9.67	83.61	
		0.55	–	–	–	0.68, 0.65	9.67	83.61	
		0.58	–	0.78	0.79, .79	0.72	9.30	84.46	
		0.59	–	0.77	0.87, 0.84	0.77	11.75	107.27	
		0.59	–	0.67	–	.76	15.48	142.47	
AFAK-4	0.5	0.17	–	1.0	–	–	9.78	83.21	76.2
B = 12.7 mm		0.18	–	1.0	0.85	–	10.06	84.17	
		0.20	–	1.0	0.94	–	10.73	86.73	
		0.20	–	0.47	–	0.99	21.46	173.46	
		0.48	–	1.0	0.89	0.94	9.88	79.07	
		0.49	–	1.0, 1.0, 0.85	0.95	.93, .93, 0.93	10.03	81.22	
		0.52	–	0.77, 0.67	–	0.91, 0.90	9.57	79.70	
		0.52	–	1.0	0.93	–	9.14	159.41	
		0.53		< 1.0	0.89	0.95, 0.95	19.42	164.60	

Note: All of the effective stress ratios measured are tabulated in this table. A dash line has been drawn where data was not available or interpretable.

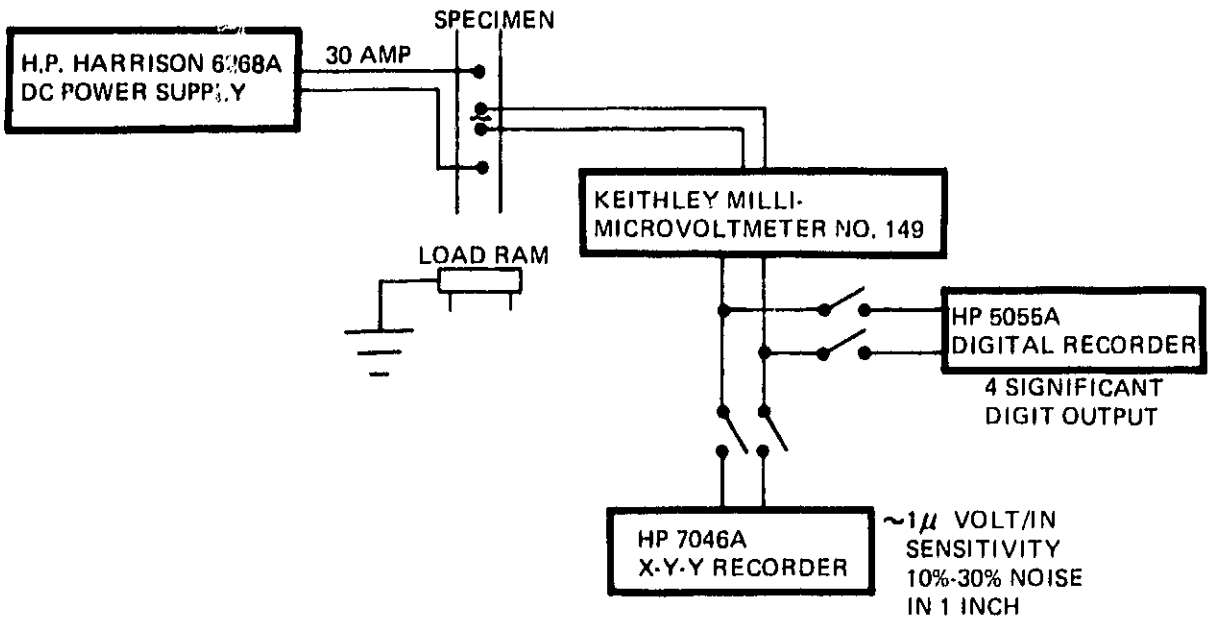

Figure 1. — Electric Potential System

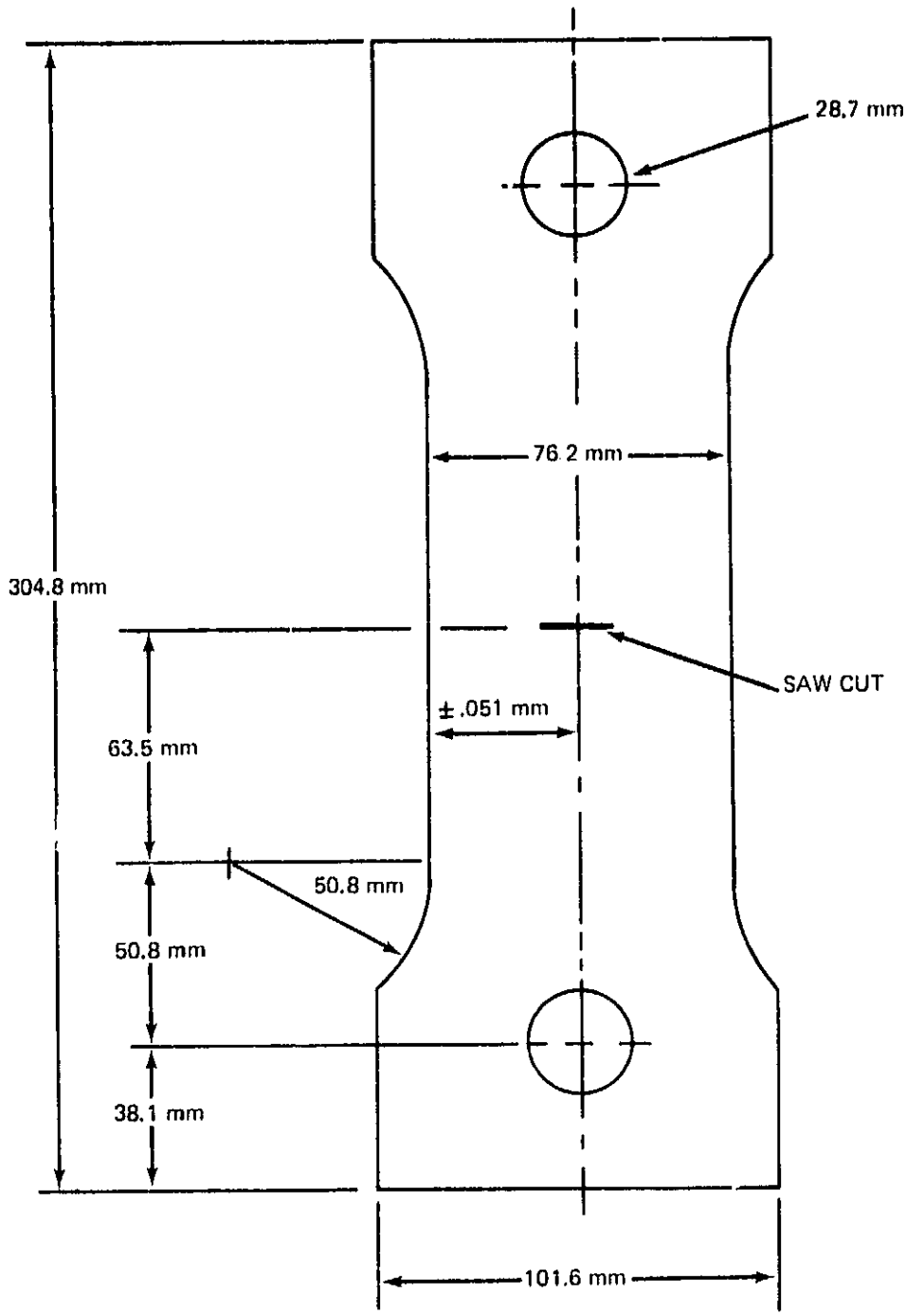

Figure 2. — Original Specimen Design

ORIGINAL PAGE IS
OF POOR QUALITY

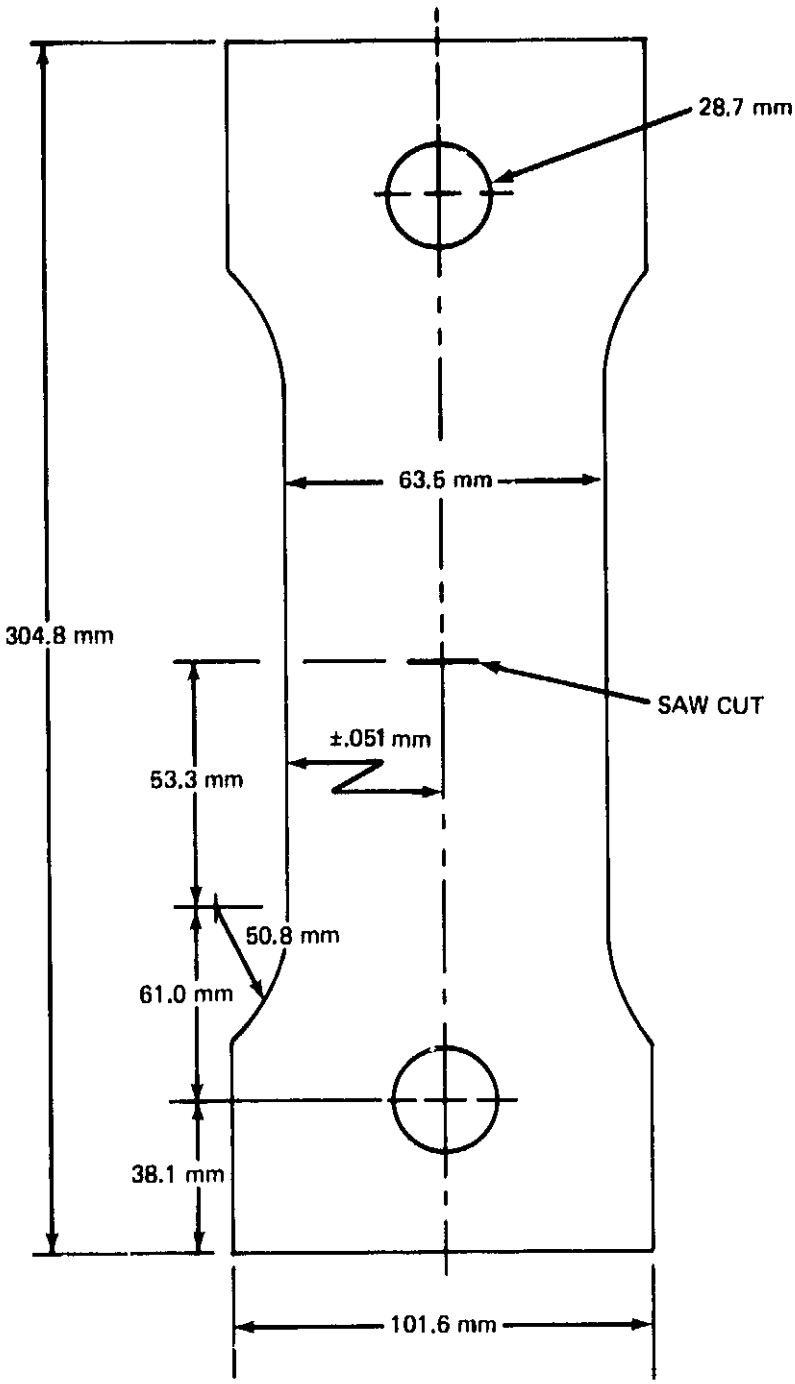

Figure 3. – Modified Specimen Design

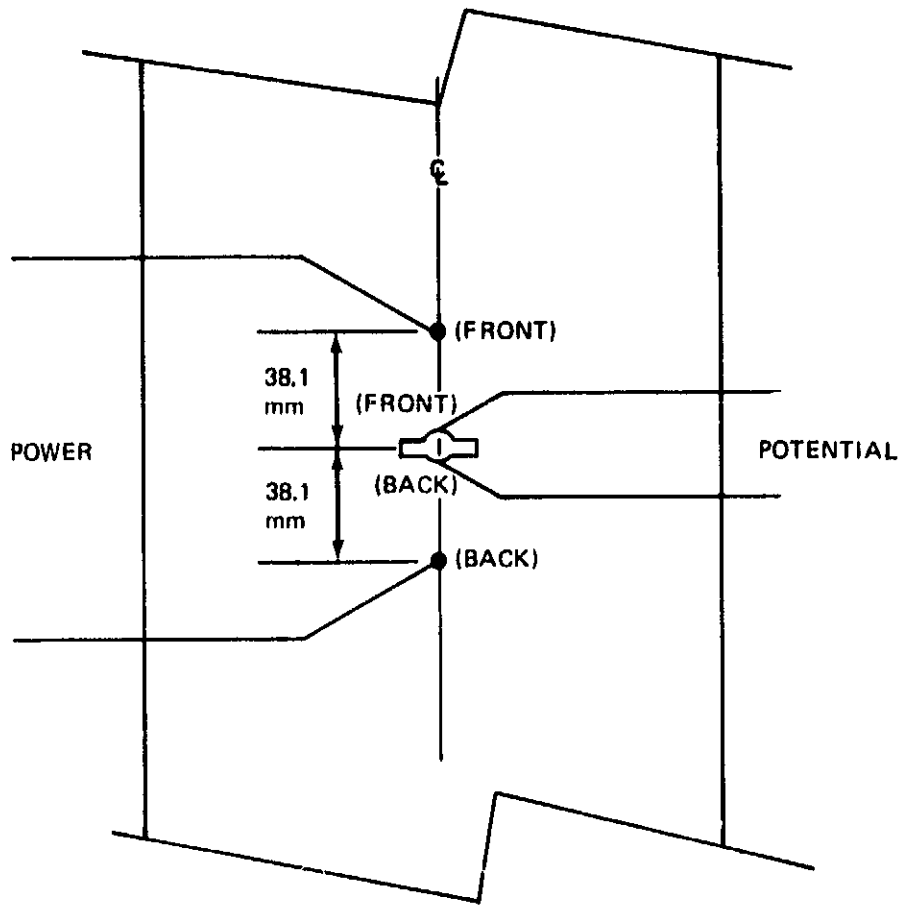

Figure 4. — Location of Specimen Power and Potential Leads

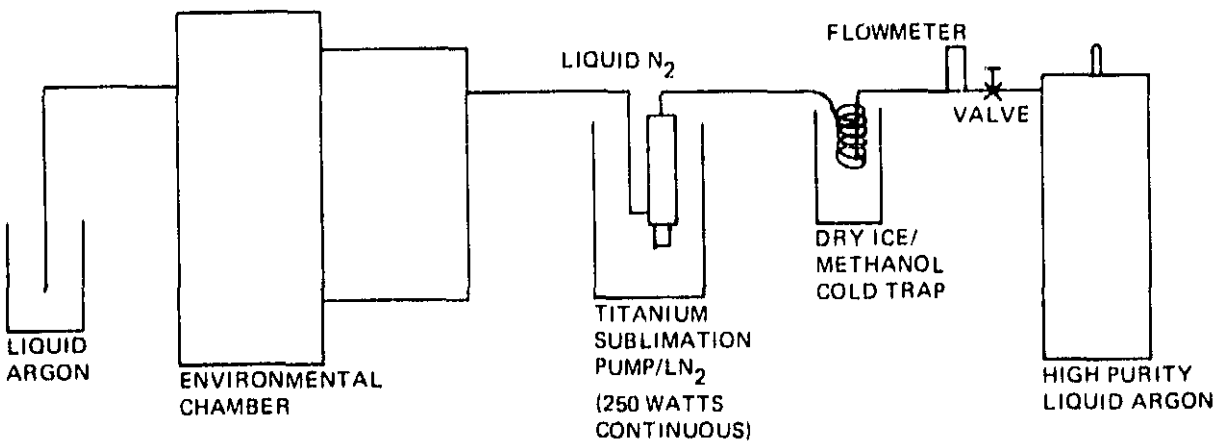

Figure 5. – Environment System Used in the Closure Study

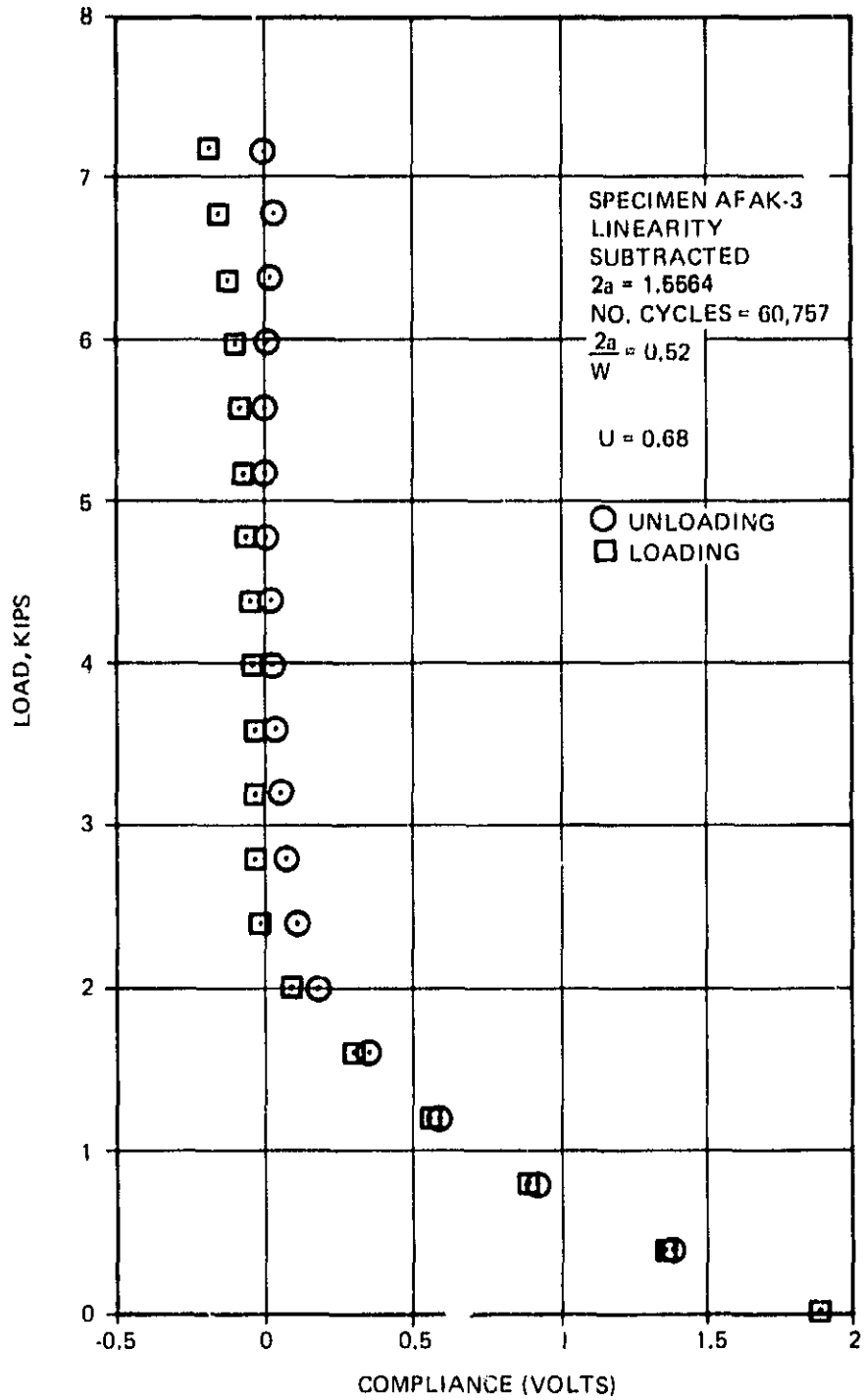

Figure 6. — Digital Compliance Data After Subtracting Elastic Unloading Slope

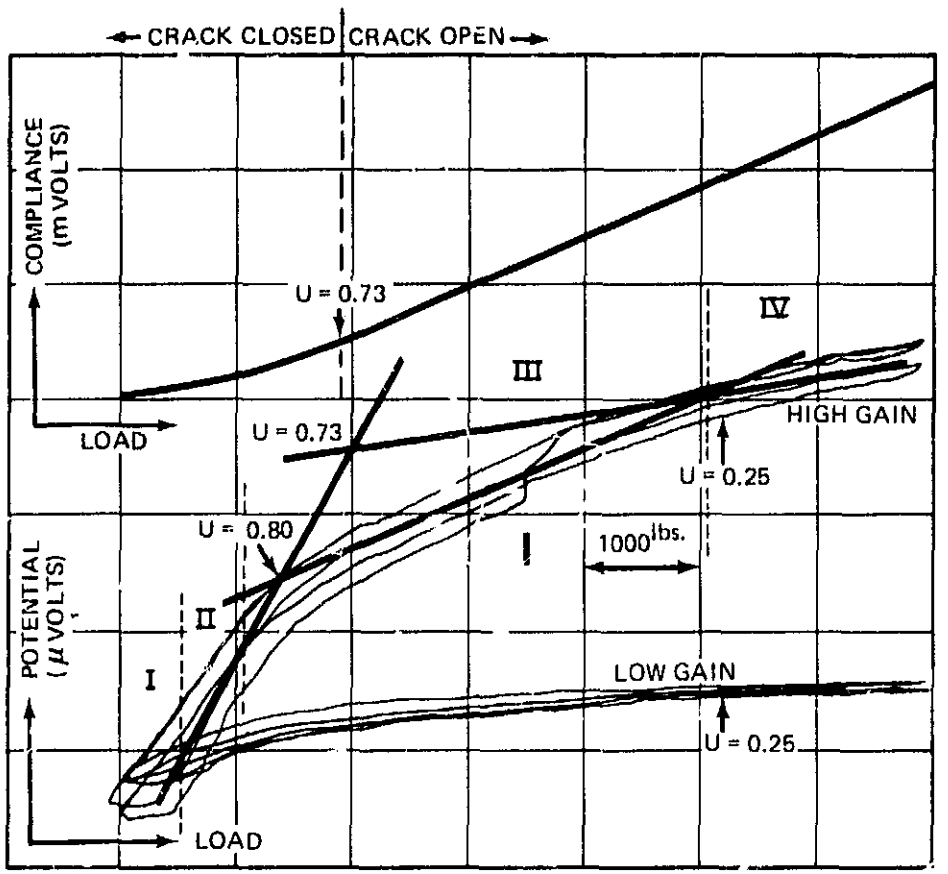

Figure 7. — Typical Compliance and Potential Data for R = 0 Specimen

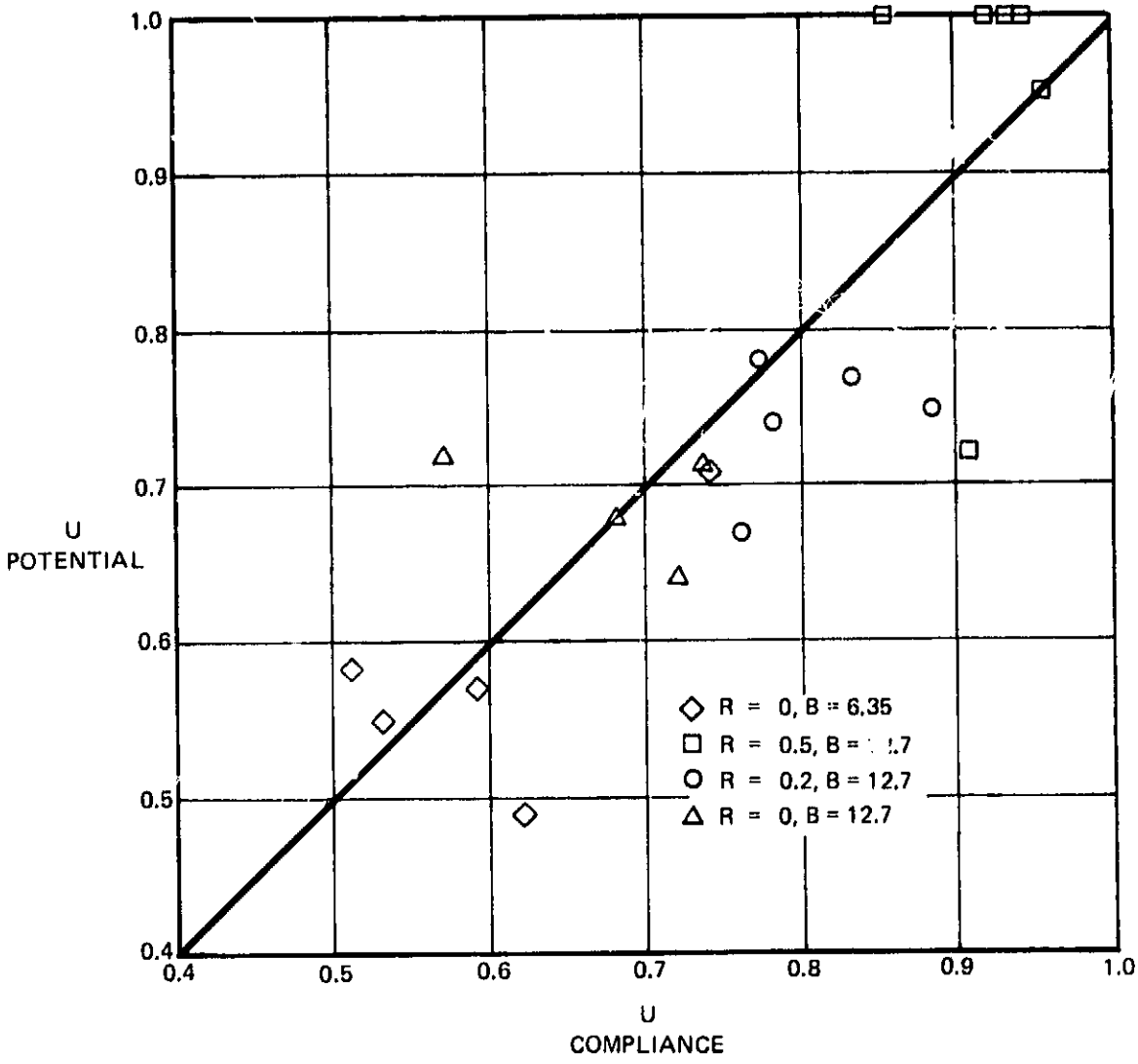

Figure 8. — Comparison of Potential and Compliance Closure Data

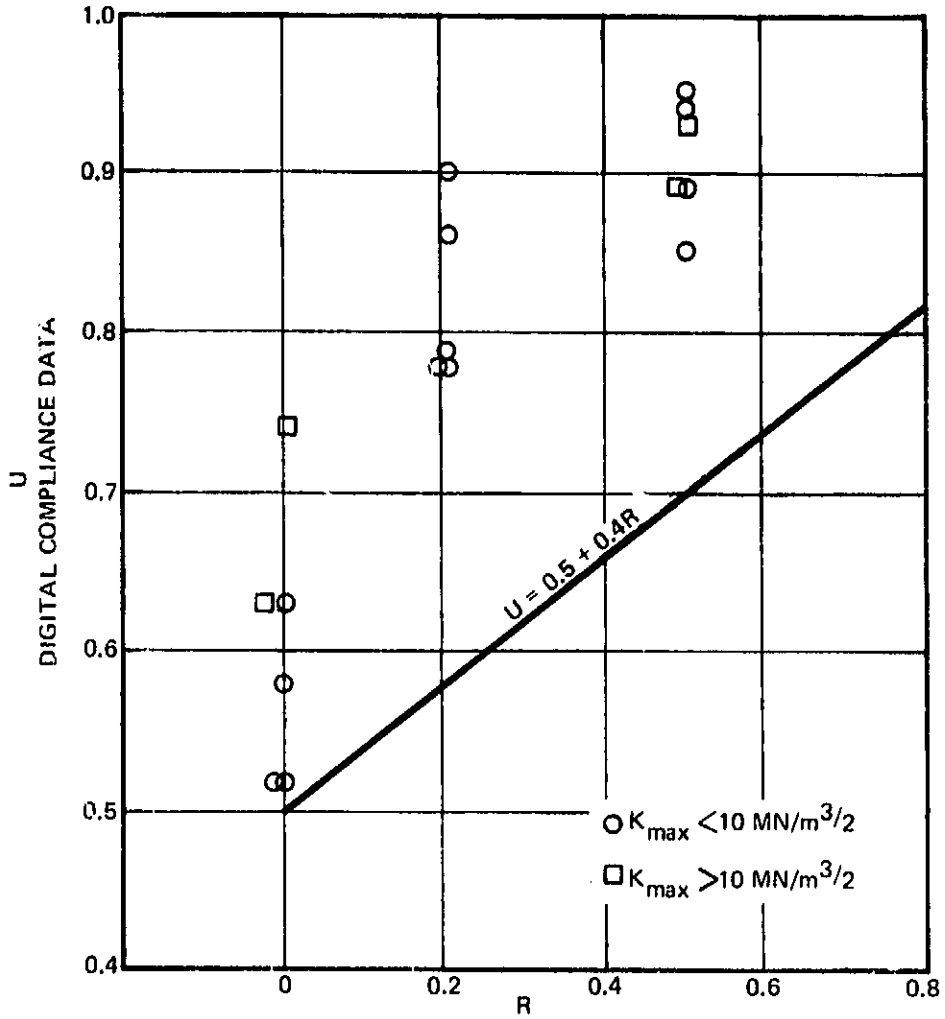

Figure 9A. – Closure as a Function of R Determined from Digital Compliance Data

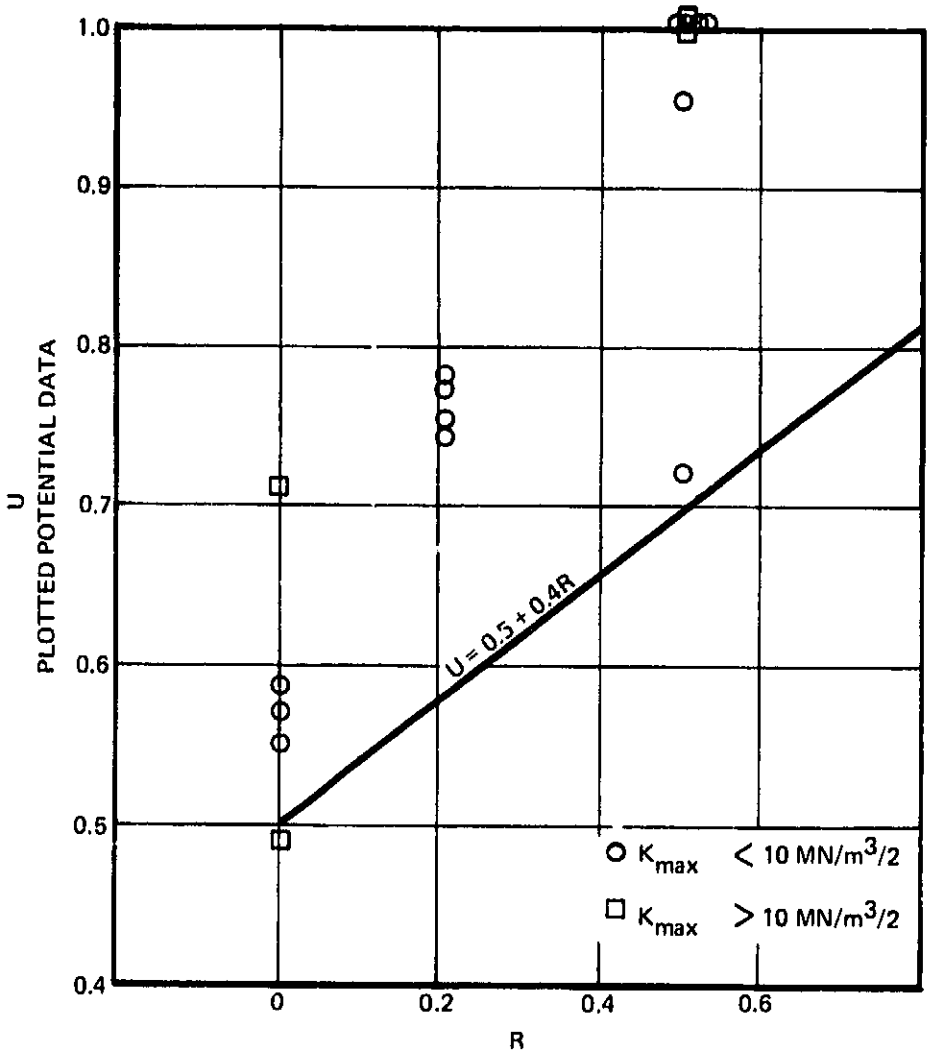

Figure 9B. – Closure as a Function of R Determined from Potential Data

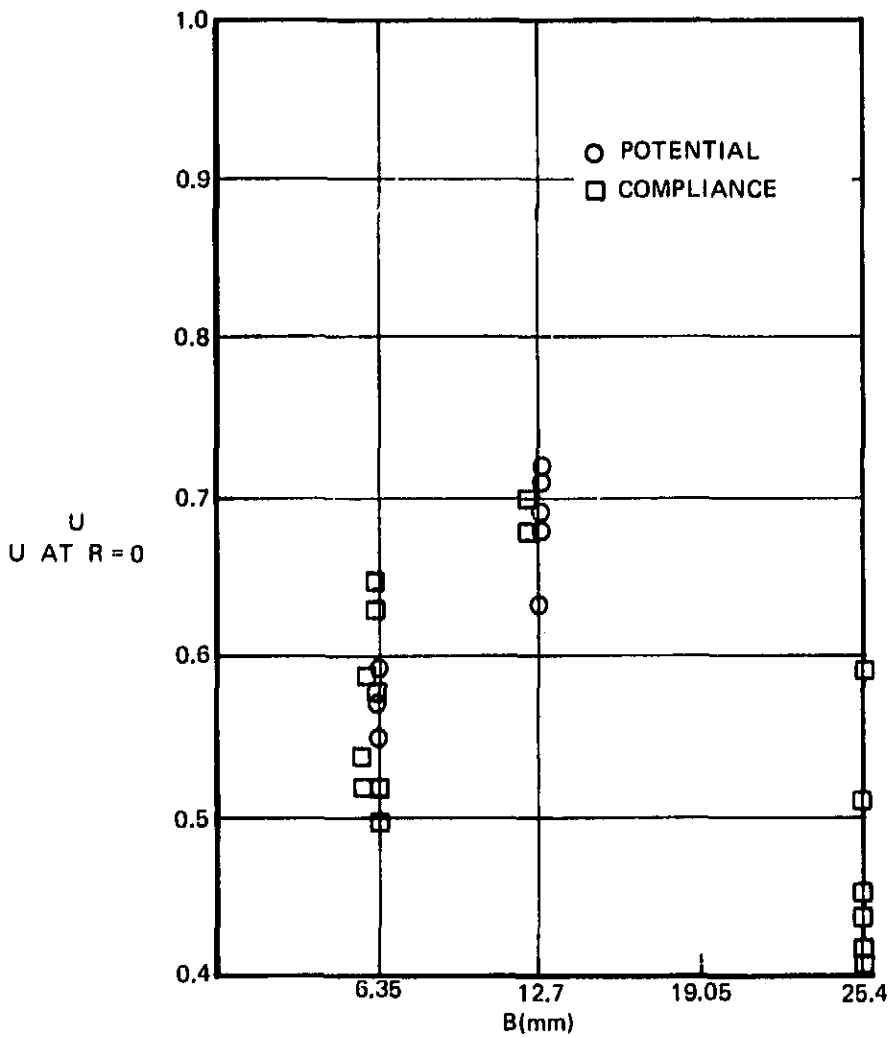

Figure 10. – Effective Stress Ratio Versus Specimen Thickness.

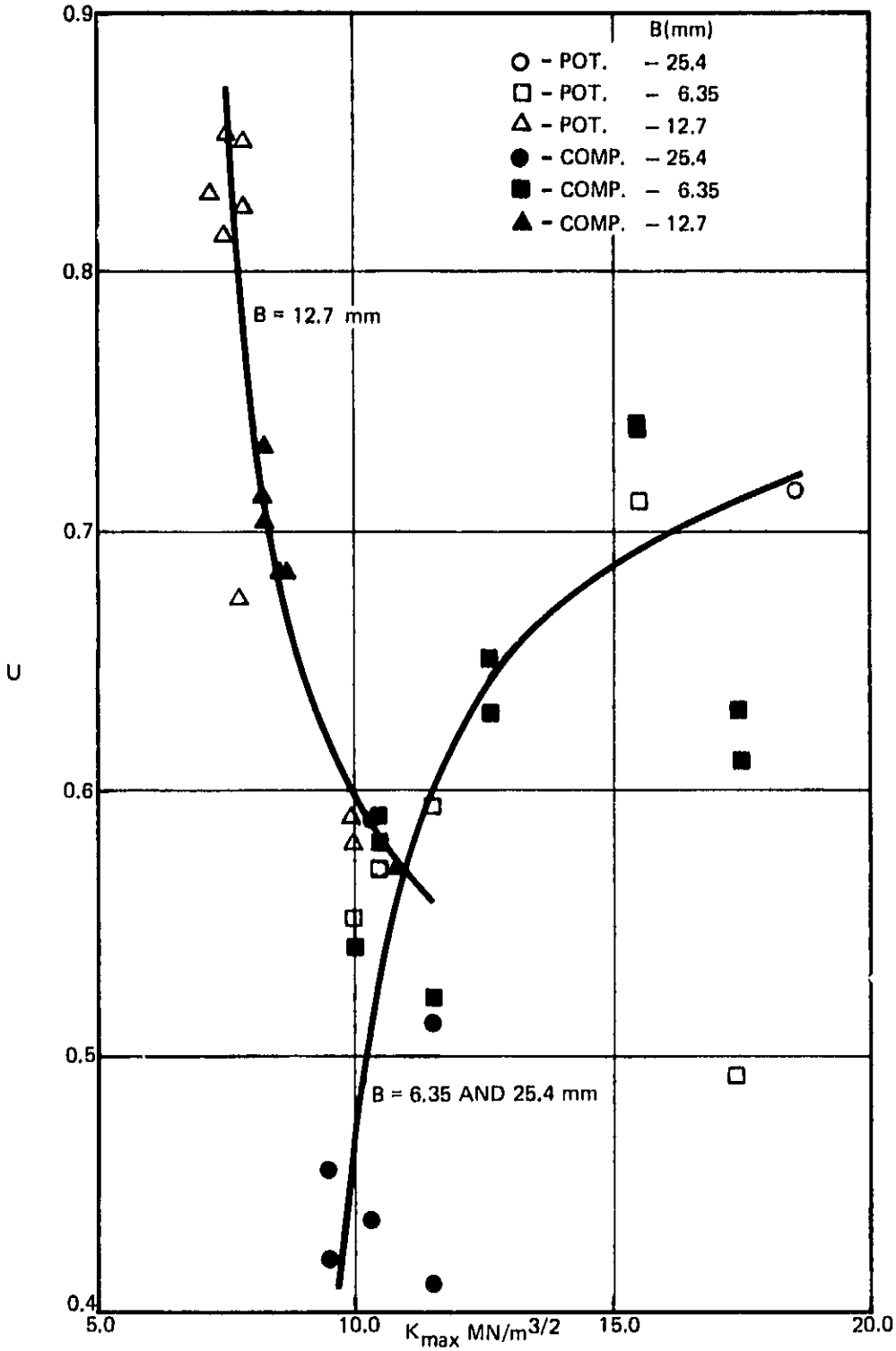

Figure 11. – Effective Stress Ratio Versus K_{max} for R = 0

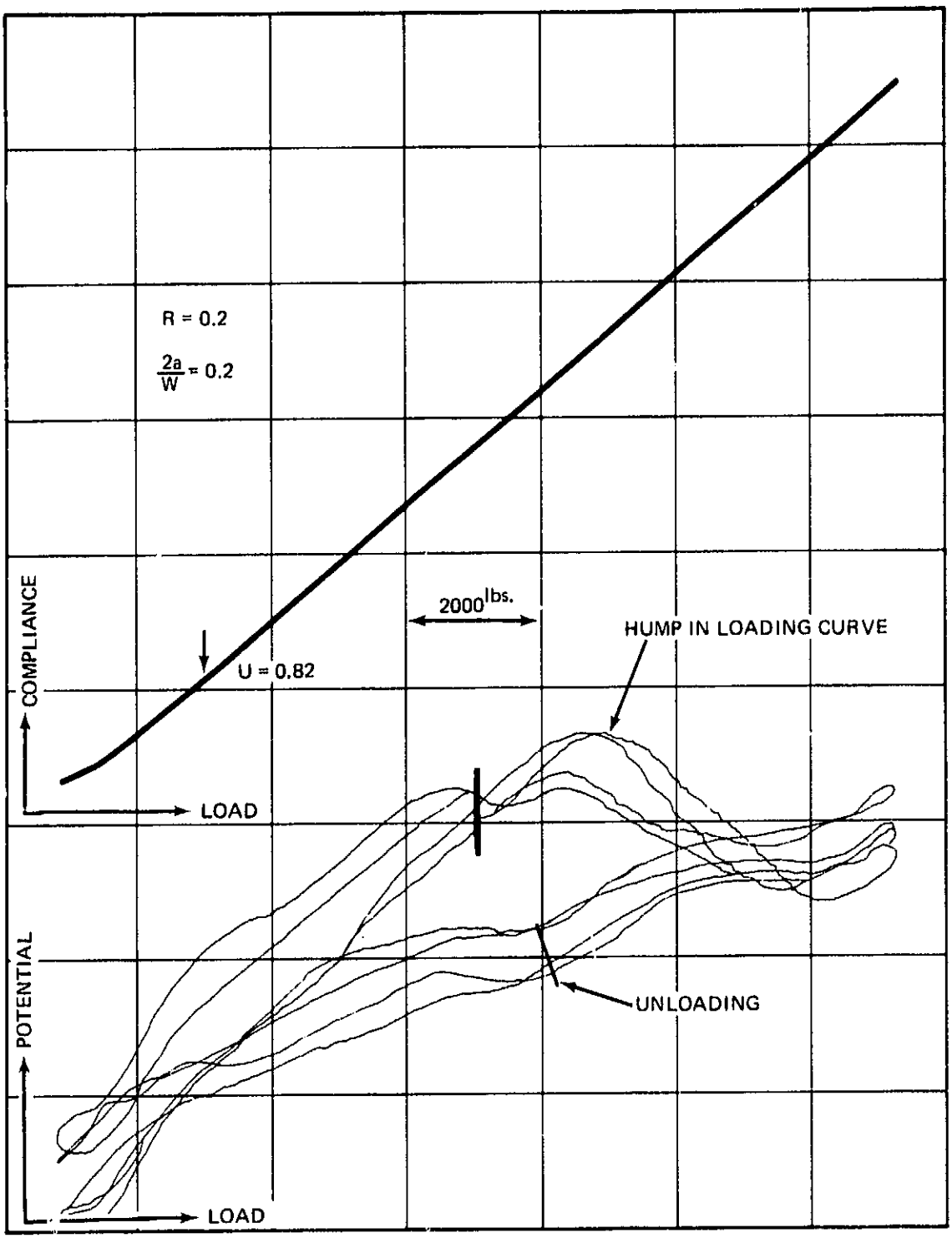

Figure 2. – Unusual Potential Behavior

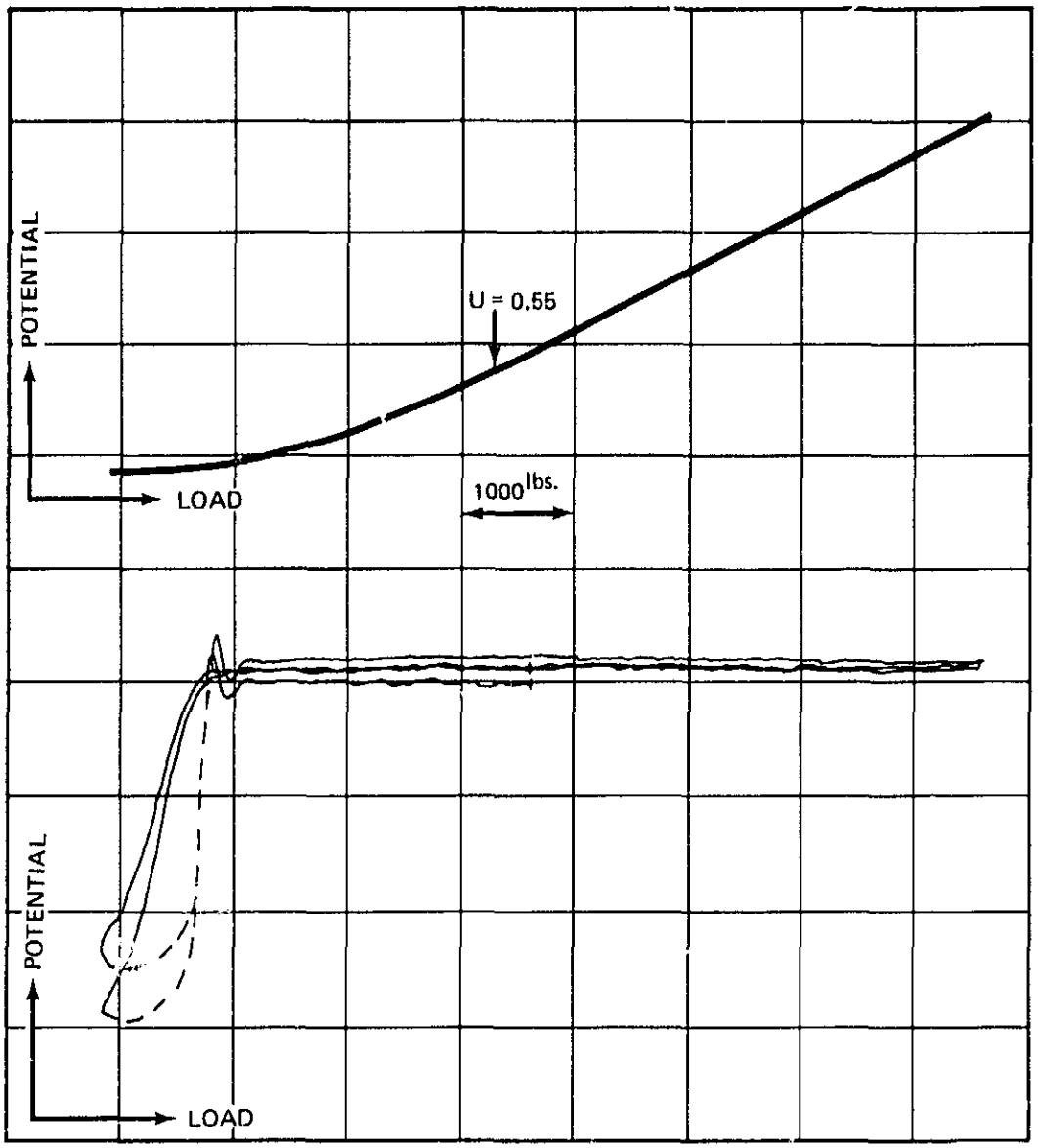

Figure 13. – Effect of Protuberance on Potential Data

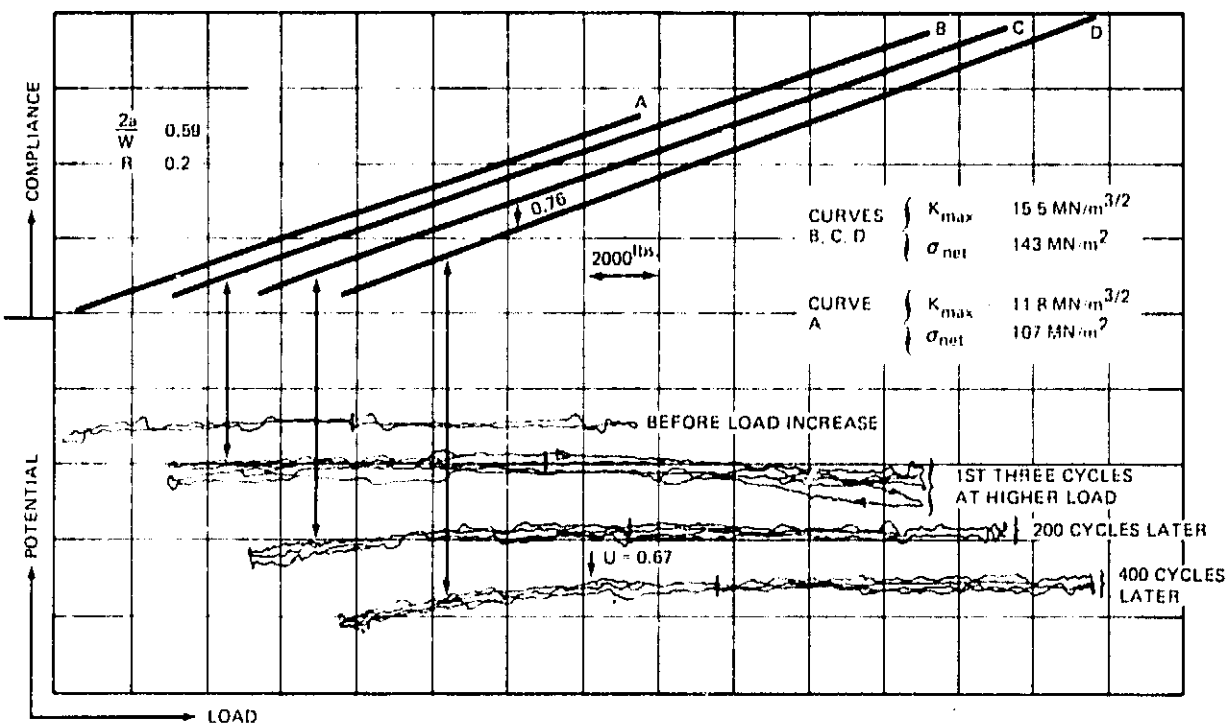

Figure 14. – Increase in Load Produced Transient Potential Response

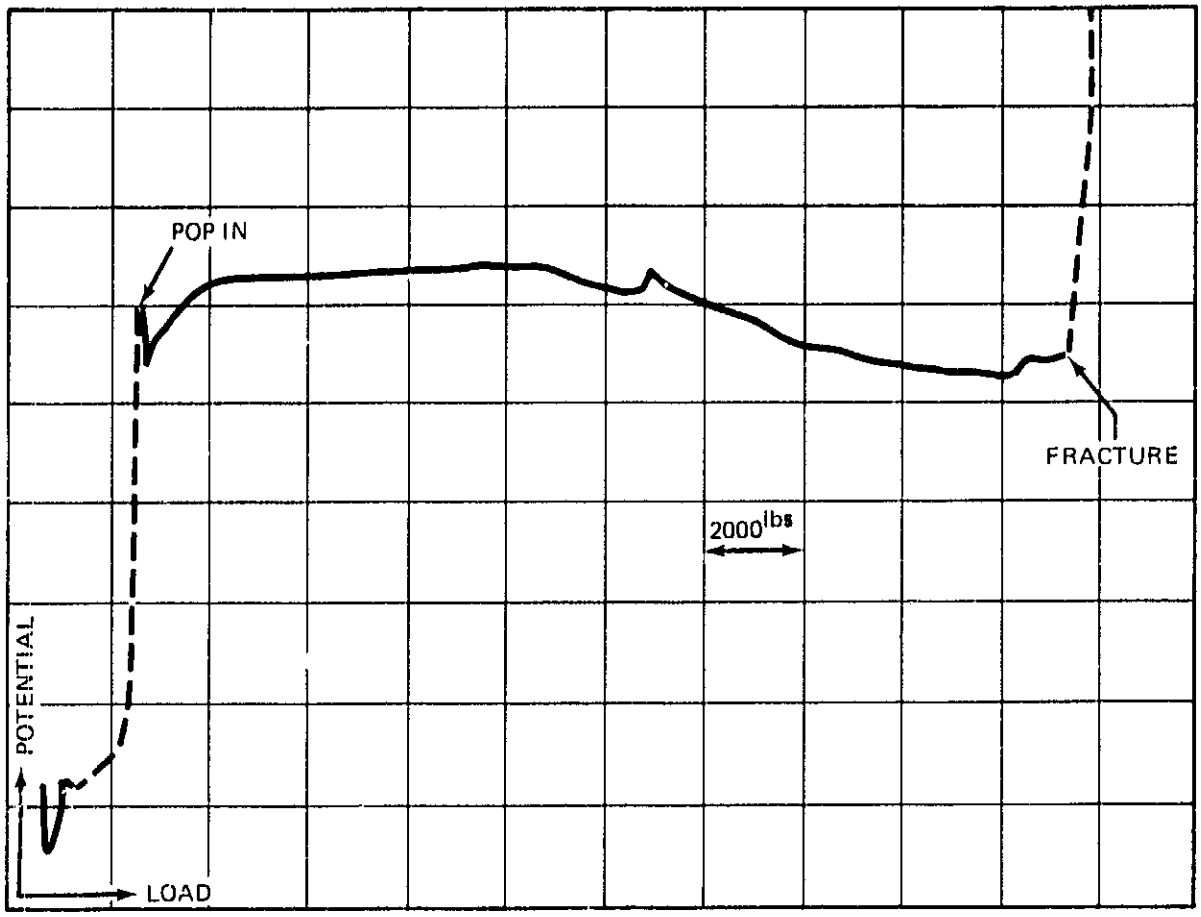

Figure 15. – Potential Versus Load Record for R = 0.2 Specimen Loaded to Fracture

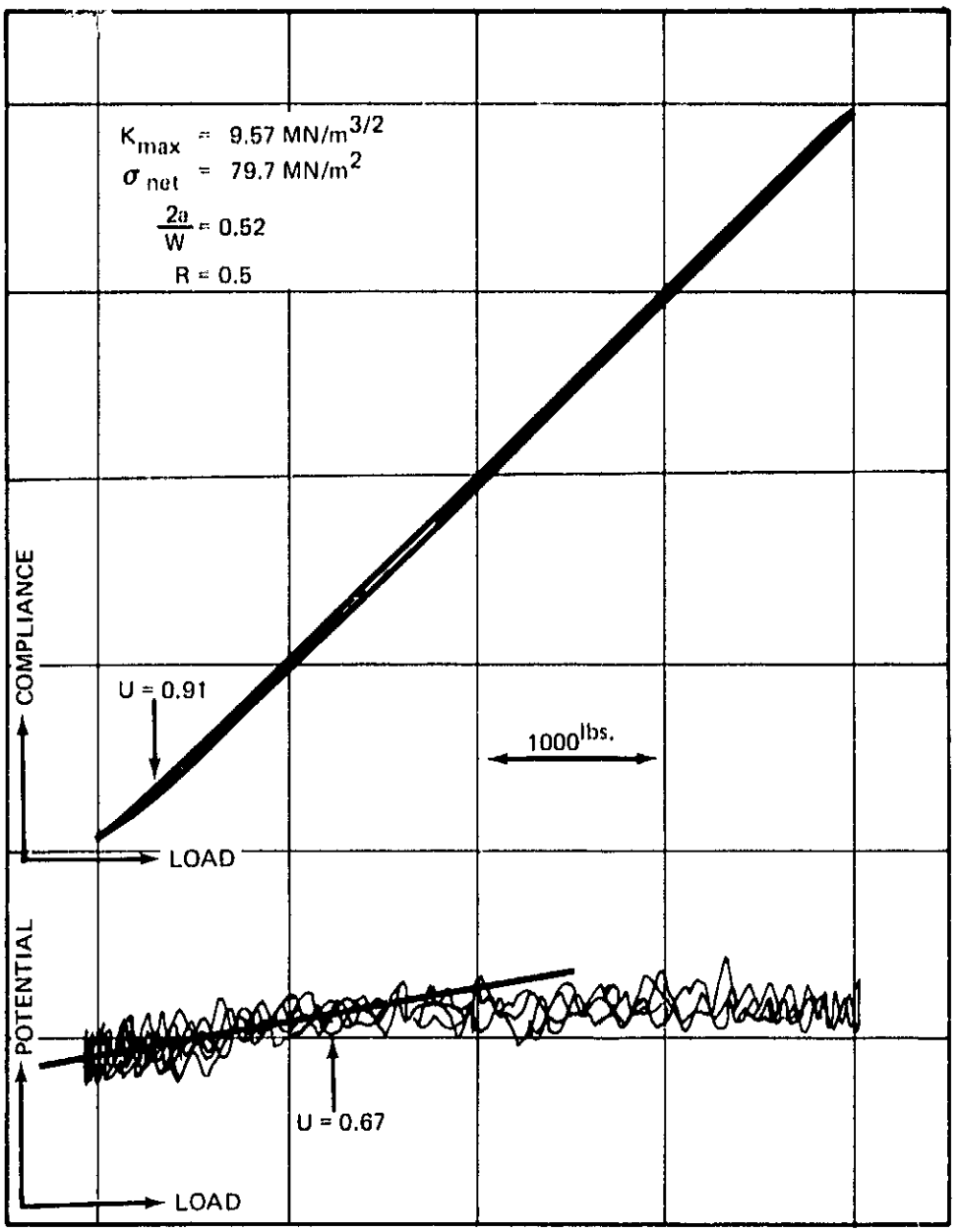

Figure 16. – Typical R = 0.5 Data

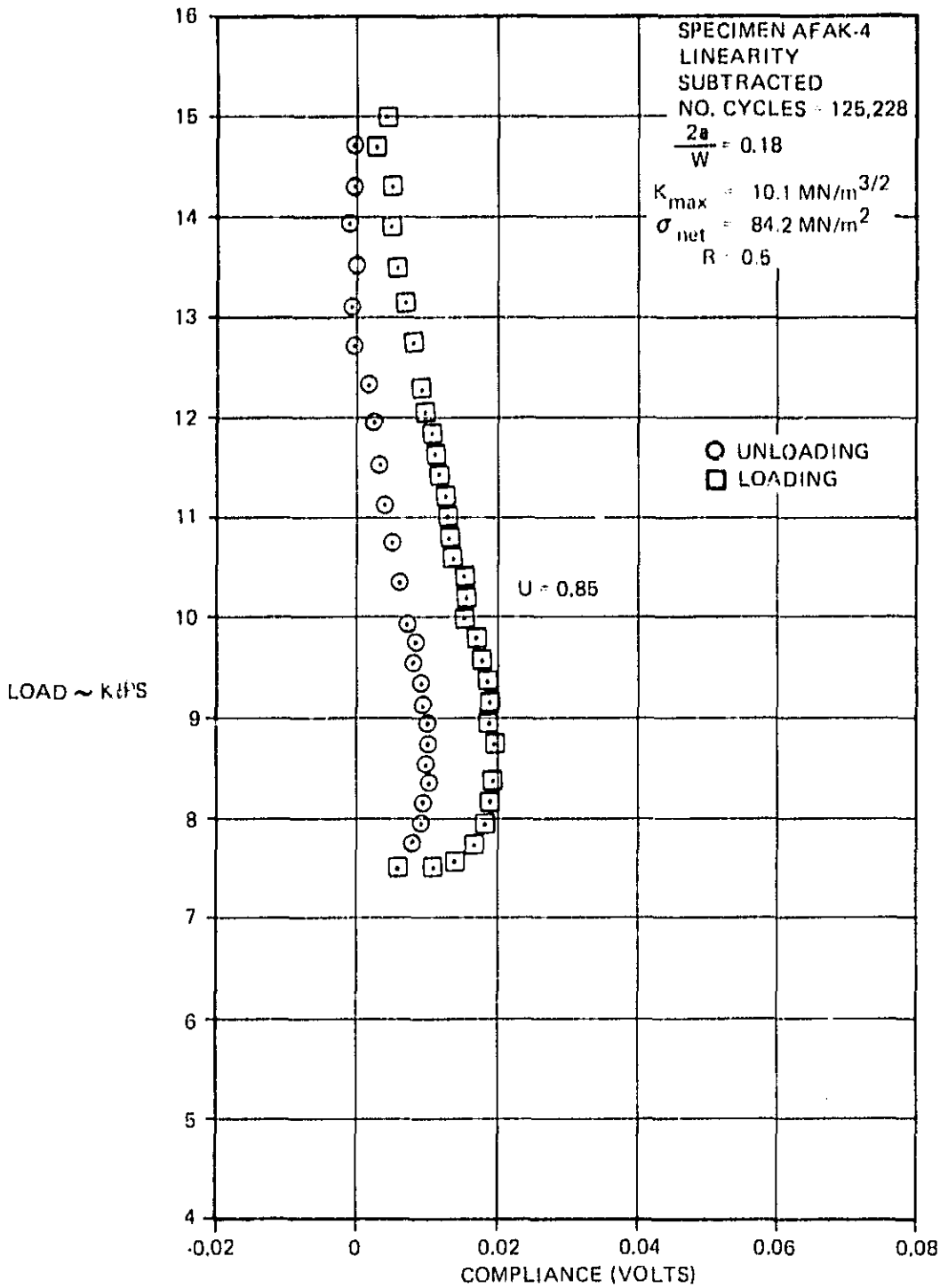

Figure 17. — Typical Digital Compliance Gage Data for R = 0.5 Specimen

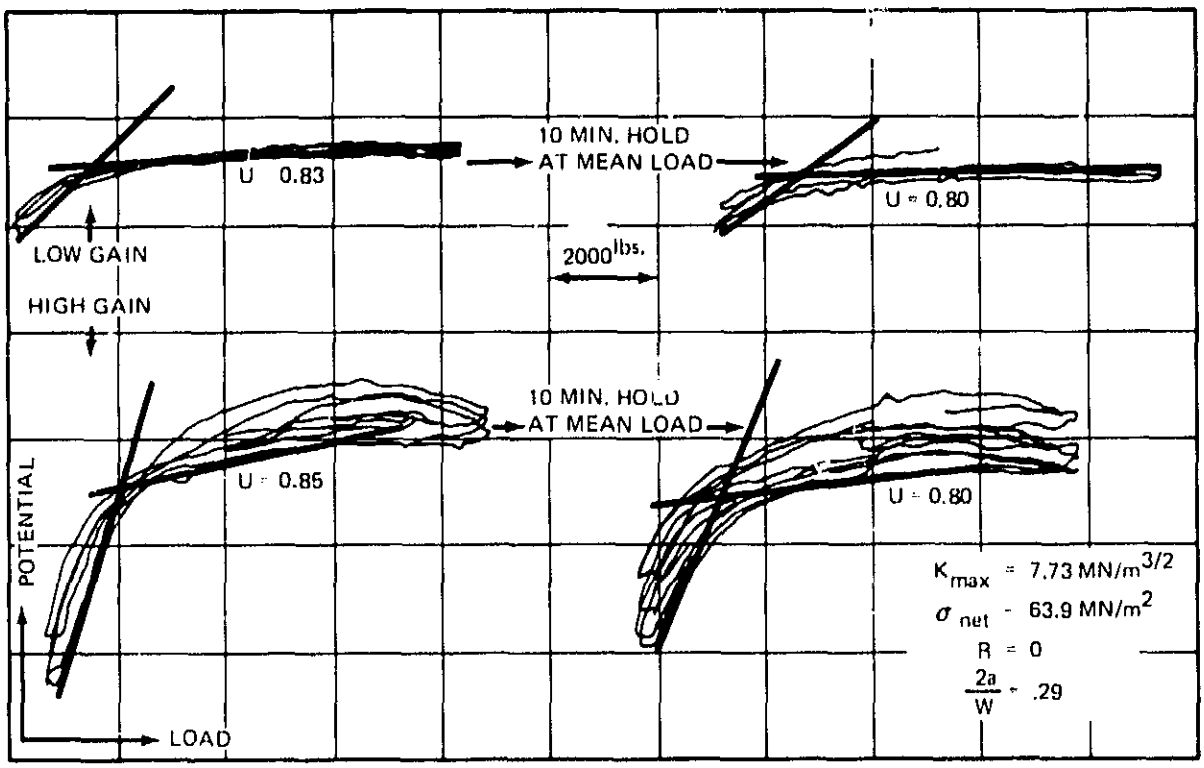

Figure 18. – Effect of Holding at Constant Load on Potential Data

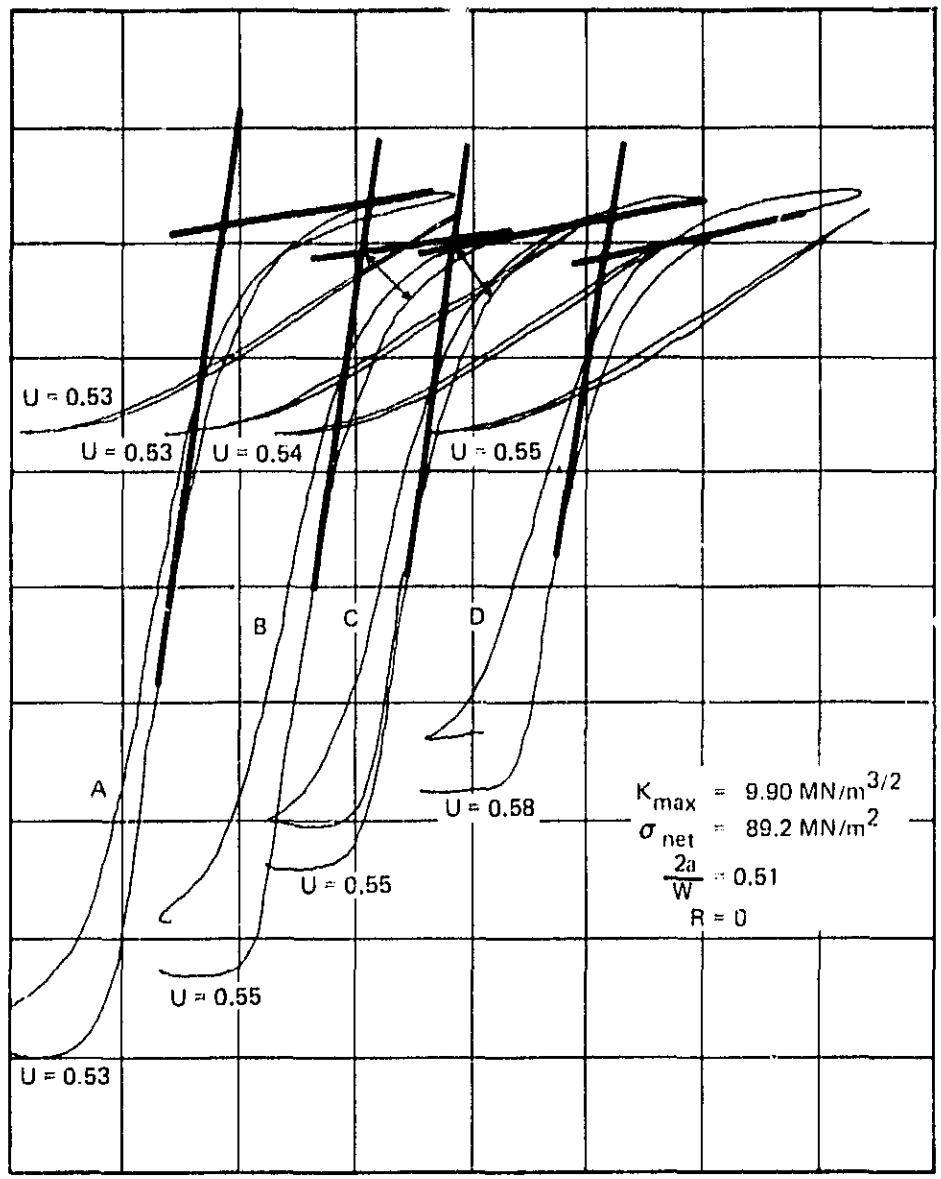

Figure 19. — Compliance and Potential Data for B = 6.35 mm Specimen

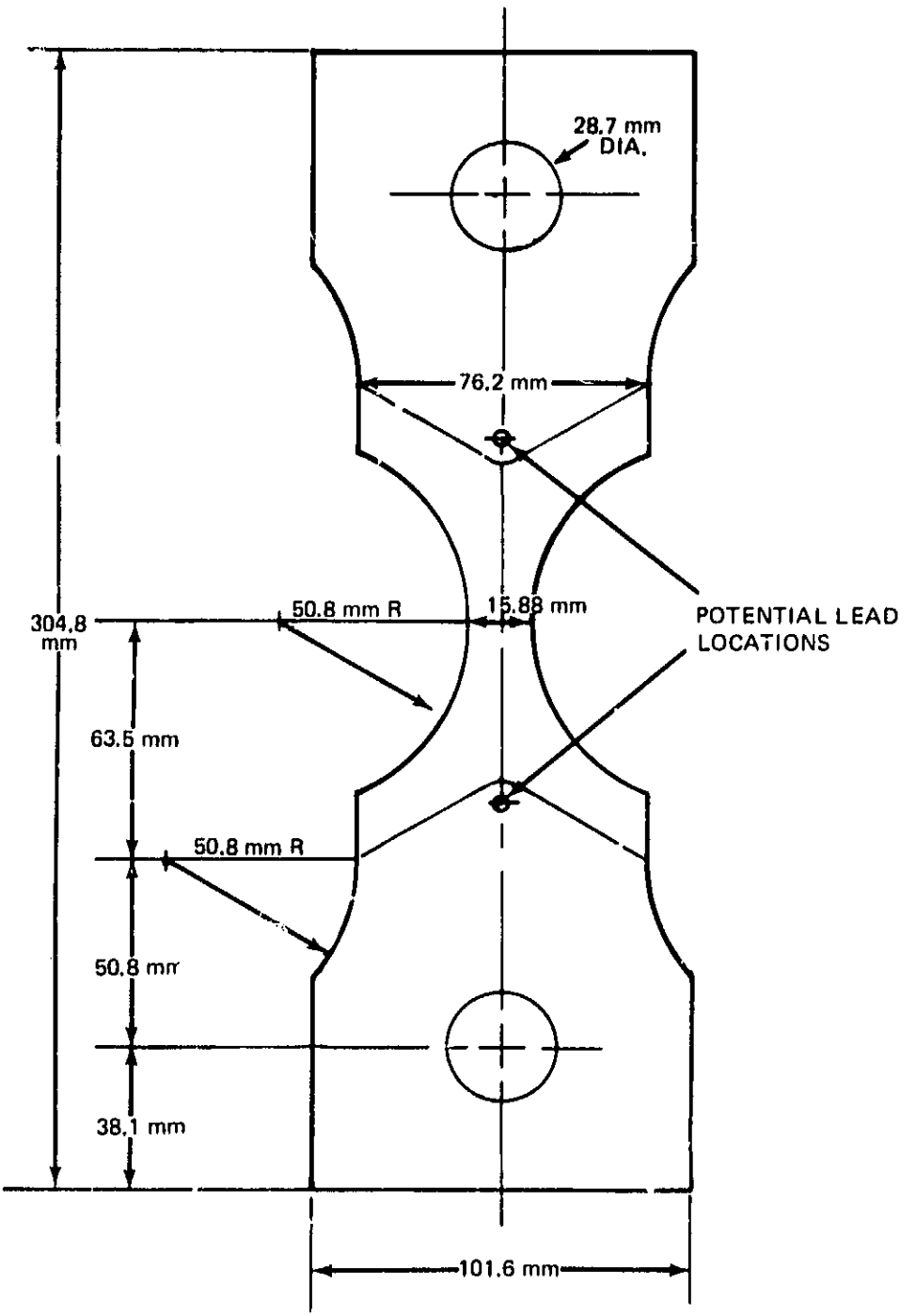

Figure 20. – Smooth Specimen Used to Investigate Response of Potential System to Plasticity

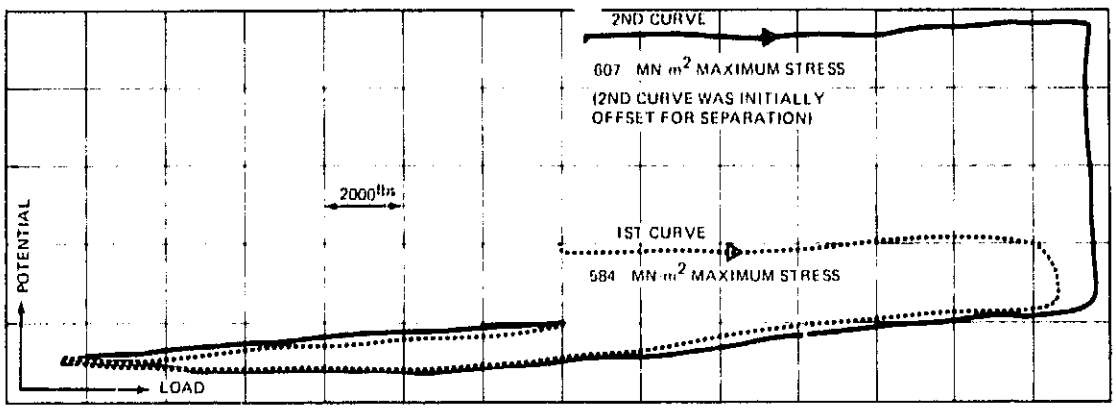

Figure 21. – Smooth Specimen Results

ORIGINAL PAGE IS
OF POOR QUALITY